jntes

JOURNAL OF NEW TECHNOLOGIES IN ENVIRONMENTAL SCIENCE

3

2021

No. 3 Vol. 5 ISSN 2544-7017 www.jntes.tu.kielce.pl Kielce University of Technology

CONTENTS

www.jntes.tu.kielce.pl
jntes@tu.kielce.pl

The quarterly printed issues of Journal of New Technologies in Environmental Science are their original versions. The Journal published by the Kielce University of Technology.

ISSN 2544-7017

Doi: 10.53412

Crossref

Valeriy DESHKO, Inna BILOUS, Dmytro BIRIUKOV

National Technical University of Ukraine "Igor Sikorsky Kyiv Polytechnic Institute", Kyiv, Ukraine

Corresponding author: biloys_inna@ukr.net

DOI: 10.53412/jntes-2021-3-1

MODELING OF UNSTEADY TEMPERATURE REGIMES OF AUTONOMOUS HEATING SYSTEMS

Abstract: *The paper analyzes the energy consumption for heating a two-room apartment based on dynamic modeling of energy processes in Matlab software environment and quasi-stationary model EN ISO 13790, which is the basis of the national standard of Ukraine DSTU B A.2.2-12:2015. A comparison of the results of modeling, taking into account the thermal interaction between the zones of the building, using a dynamic model was carried out. A comparative analysis of the installation of air temperature sensors in rooms, the signal from which is used to operate the On-Off controller, is presented. Recommendations on the installation of room temperature sensors and their number are provided.*

Keywords: *energy need for heating, controller, internal air temperature, Matlab Simulink.*

Introduction

Buildings are one of the main consumers of primary energy resources in the world. The climate conditions of Ukraine are characterized by a long heating period, which causes more than 85% of energy consumption for heating needs, a similar situation is typical for Western and Central European countries. Reducing energy consumption for heating of buildings can be achieved in various ways. One way is the use of modern insulation materials and technologies at the stages of both design and operation. The second direction is the use of renewable and alternative energy sources in distributed generation systems. The third direction is the use of automatic control of heating systems of buildings (local control of heat consumption). The fourth is the influence on the social factor, operating conditions, management of user behavior.

For qualitative evaluation and prediction of energy consumption in short time intervals, it is necessary to use dynamic calculation models [1]. There is a large number of dynamic software products, which allow estimating energy consumption of buildings, such as EnergyPlus, TRNSYS, eQuest, Matlab/Simulink, and others [1-5].

Poor regulation of indoor temperature is the most common indoor heating issue for centrally heated households in China [3]. The article [3] deals with the development of approaches for dynamic regulation of indoor temperature. The system developed in the article [3] makes it possible to provide DHS heat to a group of buildings with the same temperature demand being controlled by a single control system. However, for residents of apartment buildings with an autonomous heating system (usually a gas or electric boiler), the adjustment of automation of the heating system is carried out without taking into account several influential factors. Building Energy Management Systems (BEMS) are constantly attracting attention as an effective building control system [6, 4, 7], which requires the use of Building Energy Modeling (BEM). These systems currently work with classical control methods such as on-off, PID-control (proportional-integral-derivative controller), and optimal start-stop procedures. The thermal interaction between the different areas of the building and HVAC (Heating,

Ventilation, and Air-Conditioning) leads to different behaviors that cannot be precisely controlled by classical control methods [6]. Thus, advanced control systems that can handle multiple inputs and multiple outputs are the best approach to control the thermal condition of buildings [6-8].

In the article [9] a comparative analysis of On-Off controllers and PID-controllers used to control heat supply systems in terms of comfort conditions and energy efficiency of buildings was carried out. The research [9] showed that the use of Simulink/Matlab has a very high potential for the analysis of control strategies and for taking into account the thermal and other characteristics of the building. On-Off controllers are most commonly used because of their constructive simplicity, although great savings in energy-saving modes of operation and providing comfort conditions are better realized by PID controllers. Simulation results [9] showed that buildings with high thermal mass can significantly reduce the air temperature fluctuations in the rooms, which leads to a decrease in energy consumption. Buildings of Ukraine belong to buildings with high thermal mass.

Integration of BEM mathematical models that can describe building physics can help in successfully controlling the efficient energy consumption in buildings while ensuring comfortable conditions.

Purpose and research objectives

The purpose of the work is to analyze the energy consumption of heat energy for heating a two-room apartment using dynamic modeling, taking into account the characteristics of thermal interaction between zones (rooms).

According to the set goals, the following tasks should be solved:

1. Creation of dynamic models of the apartment with a division into zones in Matlab software environment.
2. Creation of quasi-stationary models of the apartment based on the standard DSTU B A.2.2-12:2015 [4].
3. Analysis of energy characteristics of the apartment.
4. Comparison of the calculation results in case of installation of air temperature sensors in the room, on which the controller is being operated.

Material and research results

Initial data. Existing residential housing was chosen for the study. It is a two-room apartment, located on the fourth floor of a five-story apartment building in Kyiv, built in 2016. The total area of the apartment is 49.44 m^2, the height of the walls is 2.7 m. The apartment has a window orientation to the east (E) and west (W) sides, as well as a blank outer wall oriented to the north (N). Translucent elements of the enclosures are made of metal-plastic two-chamber energy-saving double-glazed windows with argon filling of the chambers. The load-bearing part of the external wall is made of 0.4 m red hollow brick and insulated with 0.05 m mineral wool. Ventilation is natural with a multiplicity of air exchange of 0.6 $hours^{-1}$. The study used hourly climate data of a typical year of the IWEC international weather file for the Kyiv city conditions [10]. Solar heat inputs in the IWEC weather file are presented as global horizontal, diffuse horizontal, and direct normal. To recalculate the solar heat gains, which come into the area of the room, EnergyPlus software product was used, which allows taking into account the reflections of solar radiation from the surfaces of fences and soil, and take into account the optical transmittance of solar radiation, which is equal to 0.55. Figure 1 shows hourly climate data.

Model description

The apartment room was created in Matlab software environment by specifying the enclosure area and thermal resistance, which was introduced through blocks describing the convective and thermal conductivity components, as well as the heat storage properties of the internal and external envelopes,

and the air in the room. Rooms are interconnected by thermal interaction. In addition, the hourly amount of heat inputs from the sun to the area of each room and the hourly external air temperature were set. The heat source was a gas boiler in which the mass flow rate was controlled by a valve using an on/off controller, which turned on when the air temperature in the rooms fell below the specified limits and turned off when it rose above. The on/off controller has no intermediate states, either fully on or fully off. The heat output of the gas boiler is 3.5 kW, efficiency – 80%. The flow rate of the heating medium in the heating system is 0.0835 kg/s. The simulation was performed under the condition of maintaining a constant air temperature of 20°C.

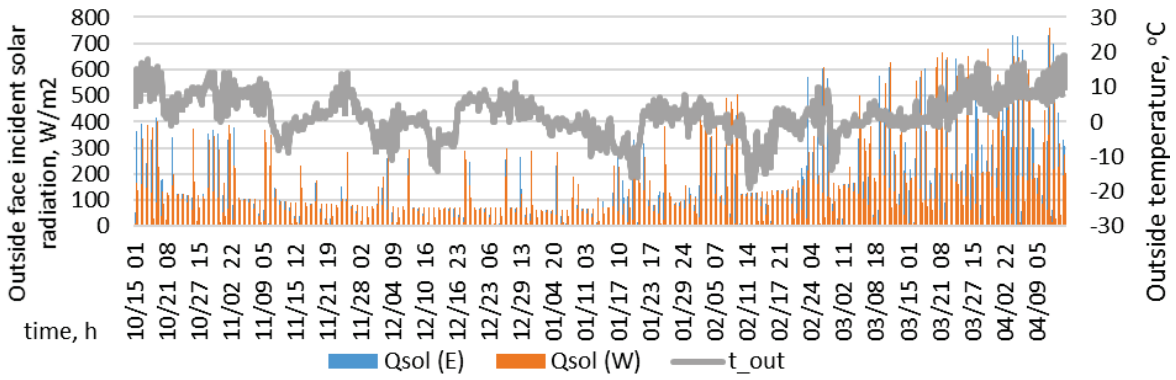

FIGURE 1. *Hourly climate data from IWEC file for Kyiv; where: t_out – outside temperature, °C; Q_{sol} – heat gain on vertical surfaces of east (E) and west (W) orientation, W/m²*

Figure 2a shows the thermal energy model of the apartment, figure 2b illustrates the thermal inertia units of one of the rooms. The step of calculating the energy demand varied automatically depending on the magnitude of changes of external and internal fluctuations of the input parameters and was in the range of 1-200 sec.

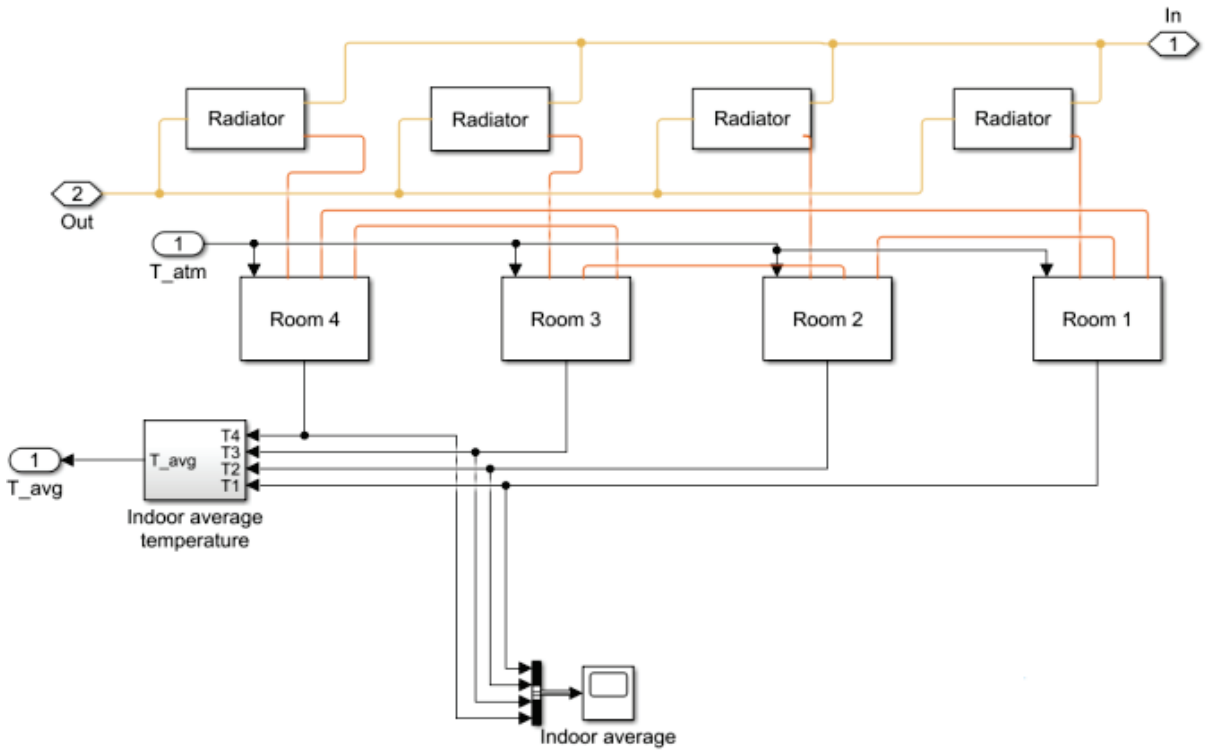

(a)

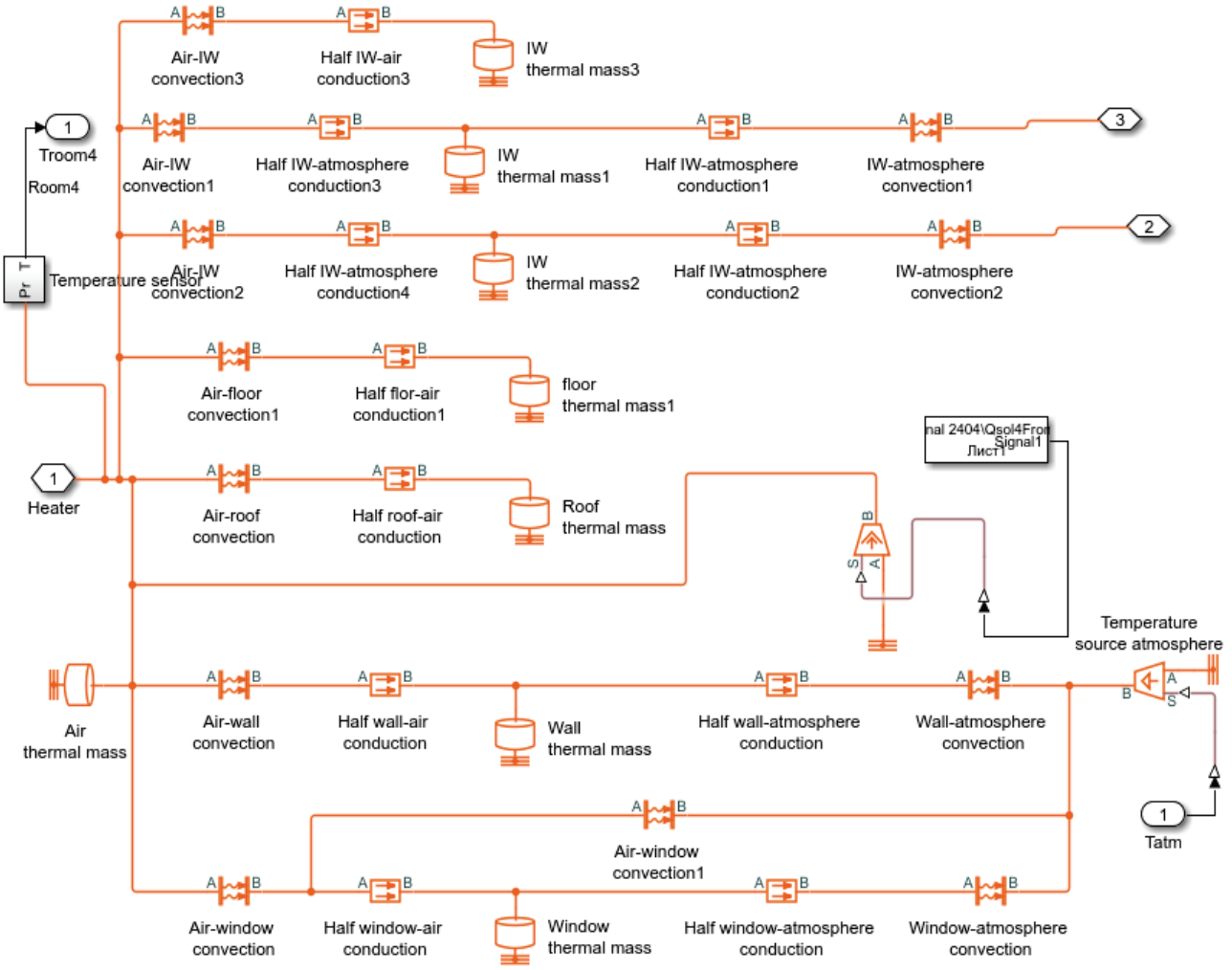

(b)

FIGURE 2. *The thermal energy model of the apartment (a) and the grid model of one of the rooms (b)*

Model testing and tuning. For the design conditions, the selection of heating devices was carried out based on a mathematical model created in Matlab software environment, where the type of heating devices, area, mass, thermal inertial characteristics of the device are taken into account. Under design conditions, following the standard [11], for the city of Kyiv, the outside air temperature is assumed to be –22°C and with no solar heat gain. The indoor air temperature, following the standard [11], is 20°C. It is determined that the capacity of heating appliances in the apartment rooms are the following: bedroom 1/room 4 – 500 W, bedroom 2/room 3 – 1200 W, kitchen/room 2 – 880 W, common areas (corridor, bath)/room 1 – 320 W.

To verify the mathematical model of the apartment created in the Matlab software environment, a comparison of the results with the quasi-stationary method according to DSTU B A.2.2-12:2015 [11]. The mathematical model based on the quasi-stationary method according to DSTU B A.2.2-12:2015 considers the apartment as a single zone and takes into account the thermal inertia properties of the external envelope only, in contrast to the mathematical model created in Matlab, which takes into account the heat storage properties of each indoor and outdoor envelope separately. The basic formulas for calculations according to the standard DSTU B A.2.2-12:2015 are given below [11].

The annual energy consumption of the house in heating and/or cooling is determined by the methodology [7]:

$$Q_o^{year} = \sum_{i=1}^{n} Q_{HC.nd.i} \qquad (1)$$

where:

i – index number of the heating month;

n – number of heating months;

$Q_{HC.nd}$ – monthly energy consumption for heating or air conditioning, W·h.

$$Q_{HC.nd} = Q_{HC.tr} + \eta_{HC.gn} Q_{HC.gn} \quad (2)$$

where:

$Q_{HC.tr}$ – monthly total heat transfer by transmission and ventilation, W·h;

$Q_{HC.gn}$ – monthly total heat gains in heating mode, W·h;

$\eta_{HC.gn}$ – dimensionless monthly coefficient of utilization of gains.

$$Q_{HC.hr} = Q_{tr} + Q_{ve} \quad (3)$$

where:

Q_{tr} – heat transfer by transmission by month, W·h;

Q_{ve} – heat transfer by ventilation, kW·h.

$$Q_{HC.gn} = Q_{int} + Q_{sol} \quad (4)$$

where:

Q_{int} – sum of internal heat gains over a given period, W·h;

Q_{sol} – sum of solar heat gains over a given period, W·h.

$$Q_{tr} = H_{hr} \left(\theta_{int} - \theta_e\right) t \quad (5)$$

where:

H_{hr} – transmission conductivity of the zone, W/K;

θ_{int} – given building zone temperature for heating, °C;

θ_e – average monthly outdoor temperature, °C;

t – duration of the month for which the calculation is performed, h.

$$Q_{ve} = H_{ve} \left(\theta_{int} - \theta_e\right) t \quad (6)$$

where:

H_{ve} – conductivity by ventilation, W/K.

The calculation to DSTU B A.2.2-12:2015 is performed for monthly intervals, i.e., only seasonal weather fluctuations are taken into account, and daily fluctuations are not taken into account. To compare the results of mathematical modeling based on the two models, weather data of a typical IWEC year [10] was used. The given values of climatic data for the monthly intervals of calculation of the heating season (October 15 – April 15) for DSTU B A.2.2-12:2015 are shown in figure 3.

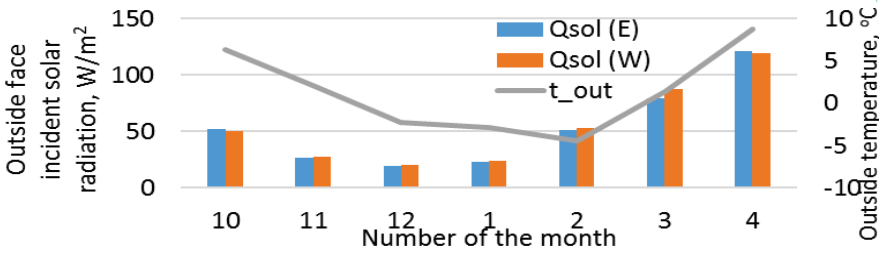

FIGURE 3. *Monthly climate data from IWEC file for Kyiv*

Analysis of the study results. Figure 4 shows the results of the simulation of heat energy consumption for heating needs. In the annual section, the difference of simulation results at constant air temperature in the apartment by the two considered models is 13%, the dynamic model created in the Matlab software environment was selected for the reference model. A smaller difference in the results is observed for the off-season period (October, April) – about 30 kWh, for other colder months it is 80 kWh, ..., 140 kWh.

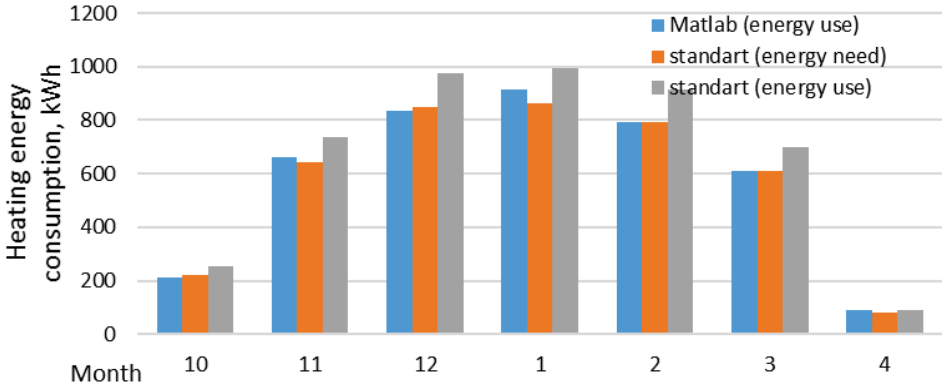

FIGURE 4. *Heating energy consumption*

From the mathematical modeling in Matlab software environment it follows that the total heat consumption of the apartment is distributed: bedroom 1/room 4 – 17%, bedroom 2/room 3 – 40%, kitchen/room 2 – 31%, common areas (corridor, bath)/room 1 – 12%. In bedroom 1, bedroom 2 steel radiators are installed, in the kitchen – steel radiator and water heated floor, in common areas – water heated floor and heated towel rail.

It should be noted that the boiler is controlled by the average air temperature in the rooms of the apartment, i.e. the boiler operates at a constant flow rate, and depending on the conditions, it changes the temperature of the water supply, thereby leading to a situation where the hourly air temperature in different rooms under the influence of, primarily, different heat gains varies from 18°C to 24°C, while maintaining the average air temperature at 20°C ±0.5°C (fig. 5).

In real-world practice, the control of maintaining the specified air temperature in the apartment is carried out by the air temperature values in the representative rooms, for small-sized typical housing, there are usually 1-2 points of installation of air temperature control sensors, according to the readings of which the controller sends a signal to the boiler to turn it on/off. Typically, the sensors are installed in the rooms where the residents are staying most of the time, i.e. in bedrooms or a living room. Three different options for installing temperature sensors are considered, as follows: 1) two sensors in bedroom 1 and bedroom 2; 2) in bedroom 1; and 3) in bedroom 2. The results of the model calculation show that the average air temperature in the rooms at which the controller is set up is: sensors in all the rooms – 19.9°C; sensors in bedroom 1 and 2 – 20°C; bedroom 2 – 19.9°C; bedroom 1 – 20.1°C. Under these control conditions, the average load on the gas boiler is: the sensors in all rooms – 954 watts; in bedroom 1 and 2 – 945 watts; in bedroom 2 – 976 watts; in bedroom 1 – 902 watts. Figure 5 shows the air temperature that the controller is outputting for the various temperature sensor installation points.

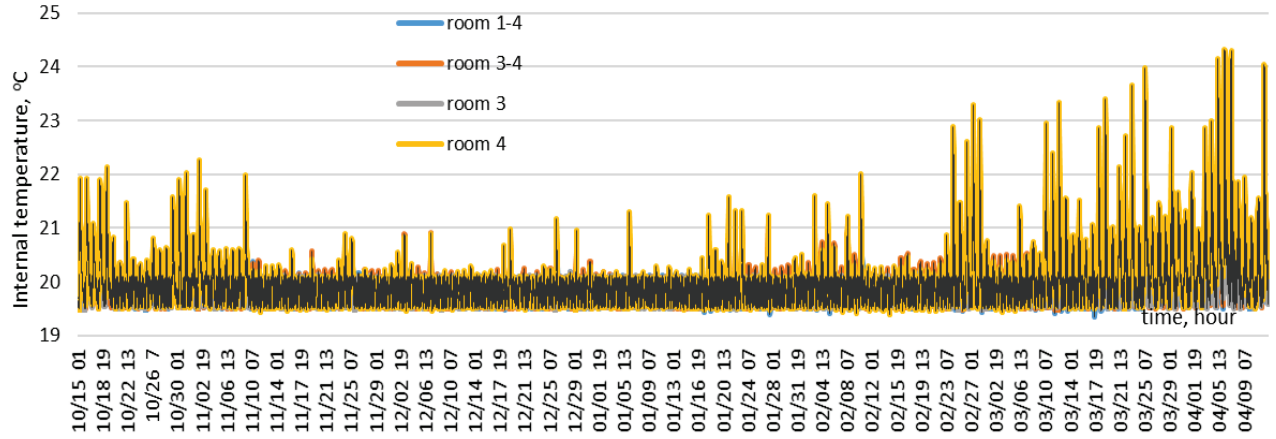

FIGURE 5. *The average air temperature in the apartment, where temperature control sensors are installed; where: room 1-4 – temperature control is based on the average temperature of all rooms; room 3-4 – based on the average temperature of bedroom 1 and bedroom 2; room 3 – based on the temperature of bedroom 2; room 4 – based on the temperature of bedroom 1*

During March-April the solar activity is high, which explains that during this period, the average air temperature in the representative rooms/groups of rooms, where sensors are installed, exceeds the value of the internal temperature change range set in the controller, that is, at the time of complete short-term heating shutdown (at times of peak solar activity) due to the excess of solar heat gain leads to an increase in indoor air temperature.

Table 1 shows deviations of the air temperature in the rooms (zones) from the average air temperature in the apartment for different locations of installation of temperature control sensors, transmitting the signal to the controller. The obtained results of the modeling show that the average air temperature in the apartment is: 1) sensors installed in all rooms (room 1-4) – 19.9°C; sensors installed in two bedrooms (room 3-4) – 19.7°C; sensor installed in room 3 – 20.2°C; sensor installed in room 4 – 19.2°C.

TABLE 1. *Deviation of air temperature in the room from the average*

Sensor installation location	Room number	Deviation from the average value, °C		
		average	max	min
room 1-4	room 1	0.3	0.9	–0.3
	room 2	–0.2	0.6	–3.5
	room 3	0.2	1.3	–1.4
	room 4	–1.1	0.1	–6.1
room 3-4	room 1	0.5	1.3	–0.2
	room 2	–0.1	1.1	–3.6
	room 3	0.4	1.7	–1.2
	room 4	–0.9	0.1	–5.7
room 3	room 1	0.0	0.4	–0.3
	room 2	–0.6	0.1	–4.2
	room 3	–0.2	0.2	–2.1
	room 4	–1.4	0.1	–6.6
room 4	room 1	1.0	2.4	–0.2
	room 2	0.5	2.5	–2.1
	room 3	0.9	3.1	–1.0
	room 4	–0.3	0.3	–4.6

The maximum fluctuations of air temperature in the rooms from the average value for the apartment as a whole are observed for the interseasonal period (March-April). The largest range of temperature fluctuations for all cases of model experiments is typical for room 4 (bedroom 1), which is caused by solar activity in the daytime hours and its absence in the dark time of the day. The rather close range of temperature deviations from the average apartment level is observed in room 3 (kitchen), which is quite close to room 4 by dimensions, amount of solar gains. Less variation in air temperature during the heating year is characteristic of room 1 (corridor and bathroom), which is explained by the absence of solar heat gain in this zone.

Figure 6 shows the energy consumption of the apartment rooms at different installation locations of the air temperature sensors, according to which the controller operates. From figure 6 it follows that with the installation of two indoor air temperature sensors in bedroom 1 and bedroom 2, the difference in energy consumption is –1.2%, in bedroom 1: –5.8%, in bedroom 2: +1.9%, as compared to the base case of calculating the installation of temperature sensors in all the rooms. The largest deviation of energy consumption for heating is obtained when the air temperature sensor is installed in room 4 (bedroom 1), which is explained by the smaller size of the room, one external wall with a large glazing factor (0.4), compared to other rooms.

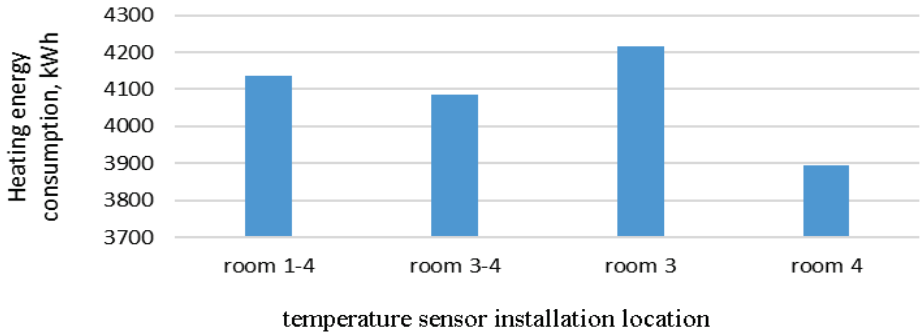

FIGURE 6. *Heat energy consumption for heating in the apartment rooms*

Conclusions

In the study, dynamic modeling of energy consumption of a two-room apartment was carried out, based on the model, created in Matlab software environment A comparative analysis of simulation results between the dynamic and quasi-stationary model has been performed. In annual terms, the discrepancy between the simulation results with the dynamic simulation created in the Matlab software environment and quasi-stationary according to DSTU B A.2.2-12:2015 is 13%. A smaller difference in the results is observed for the off-season period (October, April) – about 30 kWh, for other colder months it is 80 kWh, ..., 140 kWh. From the analysis of using different quantities and different locations of installation of air temperature sensors in the rooms, it follows that the installation of two indoor air temperature sensors in bedroom 1 and bedroom 2, the difference in energy consumption is –1.2%, in bedroom 1: –5.8%, in bedroom 2: +1.9%, as compared with the base case of installation of temperature sensors in all the rooms.

In the future, it is planned to study different types of heating system regulation settings for intermittent and continuous heating modes and to give recommendations for the installation of indoor air temperature sensors, which transmit it to the controller.

References

[1] Deshko V.I., Bilous I.Yu., Sukhodub I.O., *Mathematical models for determination of specific energy need for heating used in Ukraine*, Journal of New Technologies in Environmental Science (JNTES), 2018, No. 1. pp. 13-25.

[2] Alibabaei A., Fung A.S., Raahemifar K., *Development of Matlab-TRNSYS co-simulation for applying predictive strategy planning models on residential house HVAC system*, Energy and Buildings, 2016, No. 128. pp. 81-98.

[3] Lu G., Zhou X., Yan J., Yan G., *A temperature and time-sharing dynamic control approach for space heating of buildings in district heating system*, Energy, 2021. Vol. 221.

[4] Perera D.W.U., Winkler D., Skeie N.-O., *Multi-floor building heating in MATLAB and Modelica environments*, Applied Energy, 2016, Vol. 171, pp. 4-57.

[5] Deshko V., Buyak N., Bilous I., Voloshchuk V., *Reference state and exergy based dynamics analysis of energy performance of the "heat source – human – building envelope"*, Energy, 2020, Vol. 200.

[6] Perera D.W.U., Halstensen M., Skeie N.O., *Prediction of space heating energy consumption in cabins based on multivariate regression modelling*, International Journal of Modeling and Optimization, 2015. Vol. 5, No. 6, pp. 385-392.

[7] Perera W., Pfeiffer C.F., Skeie N.O., *Modeling and simulation of multi-zone buildings for better control*, 55th Conference on Simulation and Modelling, 2014, Aalborg, Denmark, Linköping University Electronic Press.

[8] Perera D.W.U., Pfeiffer C., Skeie N.O., *Control of temperature and energy consumption in buildings*, International Journal of Energy and Environment, 2014, Vol. 5, No. 4, pp. 471-484.

[9] Saleh A., Mosa M., *Analysis of control strategies and simulation of heating systems using Simulink/Matlab potential*, Journal of Thermal Engineering, 1 October 2016, Vol. 2, Issue 5, pp. 921-927.

[10] International Weather for Energy Calculations, https://energyplus.net/weather-location/europe_wmo_region_6/UKR.

[11] Enerhetychna efectyvnist budivel. Metod rozrahunku enerhospozhyvannia pry opalenni, okholodzhenni, ventyliatsii, osvitlenni ta hariachomu vodopostachanni/DSTU B A.2.2-12:2015 (Natsionalnyi standart Ukrainy), K.: Minrehion Ukrainy, 2015, p. 203.

Victor WYSOCHIN, Vladimir NIKULSHIN, Alla DENYSOVA

State University "Odessa Polytechnic", Ukraine

DOI: 10.53412/jntes-2021-3-2

INFLUENCE OF THE COOLANT FLOW RATE ON THE TEMPERATURE CONDITIONS OF THE HYBRID PV MODULE OPERATION

Abstract: *Numerical researches of thermal regimes of a hybrid photovoltaic-thermal panels (PVT) for refrigerating conditions which are discriminated by way of a problem of the charge of heat-transfer agent are conducted. Two typical refrigerating duties PVT are observed, first of which is characterised not connected with sizes of an absorber the heat-transfer agent charge; second – a choice of the charge of heat-transfer agent depending on the absorber square. The work purpose – creation of a method of definition of temperature characteristics of thermal regimes for their rationalisation. Features of the observed regimes are shown. Proceeding from interconnection of temperatures of an absorber of a radiant energy and chilling heat-transfer agent, for generalisation of the solution of system of the equations the temperature factor is inducted. It defines a relationship of change of temperature of heat-transfer agent and average temperature of an absorber and is a parametre of efficiency of a heat transport from an absorber to chilling heat-transfer agent. As showed the analysis, the greatest agency on heat transport efficiencyratio under constant regime conditions is rendered by intensity of irrradiation, ambient temperature and absorber sizes. At the heat-transfer agent charge, connected with the absorber area, its magnitude does not influence heat transport efficiencyratio. Generalising dependences for calculation of temperature characteristics are offered.*

Keywords*: PVT, hybrid photovoltaic thermal panel, temperature regimes.*

Introduction

It is known that efficiency of electric energy production of the photomodule depends on its temperature. To decrease the heating of device apply natural and a forced cooling. In the last case the organised remove of warmth gives the chance to its use [1–3] that raises the general power efficiency of the device. In a hybrid solar collecting system (PVT) photocells are chilled by an active cooling system of by heat-transfer fluid through channels in a back part of the module.

Brief analysis of recent publications

Producers of photomodules restrict temperature level of maintenance of photomodules in limits 45°C, ..., 50°C. However for PVT where the heat-transfer agent reheat temperature predetermines a direction of use of power resources, the thermal operating mode of the device should be proved. At sampling of temperature operating modes PVT, as a rule, use analytical models [3, 4]. Boundedness of the mathematical description on a way and detail of work of installations in interfaced and essentially variable conditions thus occurs. It complicates sampling of effective temperature operating modes PVT taking into account thermal and electric productivity at simultaneous satisfaction of the combined loading.

Goal

Working out of the integrated mathematical model for definition and rationalisation of temperature operating modes of a hybrid photovoltaic-thermal panels.

Method of investigation

For the analysis it is accepted the modelling structure of the device consisting of an absorber of solar energy which on the one hand is fenced from an outer space by a pellucid wall, with another is an element of the flat channel for chilling heat-transfer agent.

The heat transport in PVT is defined by external and internal conditions of a leakage of process. External conditions are intensity of irrradiation PVT and heat exchange with environment. Internal conditions are formed at heat exchange between an absorber and heat-transfer agent, and also between heat-transfer agent and the back wall bounding on environment. These processes are presented by system of the equations of conservation of energy:

– in an absorber:

$$H(\tau\alpha)\left(1-\eta_{ep}\right)=U_{ab-a}\left(t_{ab}-t_a\right)+U_{ab-f}\left(t_{ab}-t_f\right) \tag{1}$$

– in heat-transfer agent:

$$cg\frac{dt_f}{dx}=U_{ab-f}\left(t_{ab}-t_f\right)-U_{f-w}\left(t_f-t_w\right) \tag{2}$$

– in a back wall of the channel:

$$U_{f-w}\left(t_f-t_w\right)=U_{w-a}\left(t_w-t_a\right) \tag{3}$$

where:

H – density of a quantity of radiant energy;
$(\tau\alpha)$ – reduced adsorption capacity of solar collector;
η_{ep} – efficiency ratio of transformation of solar energy in the electric;
t – temperature;
U – heat transfer coefficient;
g – heat-transfer agent mass flow rate;
a – ambient;
ab – absorber;
f – fluid;
w – back wall.

Value of efficiency ratio of transformation of solar energy η_{ep} depends on temperature [4]:

$$\eta_{ep}=\eta_{\text{maxSC}}\left[1+\alpha_P\left(t_{ab}-t_{\text{SC}}\right)\right] \tag{4}$$

where:

η_{maxSC} – efficiency ratio of transformation of solar energy photopanal in a point of the maximum power under standard conditions (SC);

t_{SC} – temperature panal at the SC;

α_P – temperature power factor cell, K^{-1} .

The system of the equations which includes on the equations in the algebraic and differential aspect, added with boundary conditions, characteristic for maintenance of solar devices, dared a numerical

method. As change of temperatures in system occurs along a heat-transfer agent current, we make rationing of observed parametres concerning a channel width. Thus we gain that for the absorber area in characteristic functional parametre the length of the channel is.

Study results and their discussion

By consideration of the combined power device by analysis key parametres heat exchange processes the outlet temperature of heat-transfer agent and absorber temperature are. Observed parametres essentially change along an absorber surface as it is visible on figure 1, where it is shown a dynamics of characteristic temperatures PVT along the channel in conditions typical for such device. These are condition assumes working out simple in use of algorithm of definition of such temperatures. Recognising that presented on figure 1 dependence it is close to linear, in the capacity of settlement temperature of an absorber its arithmetic-mean magnitude can be accepted ($\overline{t}_{ab}$).

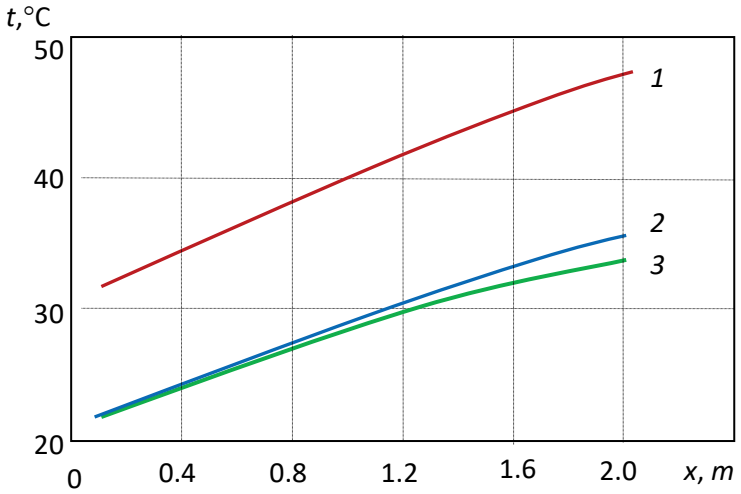

Figure 1. *Change of characteristic temperatures along the stream (coordinate x): 1 – heat-transfer agent; 2 – an absorber; 3 – an outdoor wall*

Let's observe two refrigerating duties PVT:

- first – not connected with sizes of an absorber the heat-transfer agent charge, $g \neq f(A_{ab})$;
- second – at the heat-transfer agent charge, chosen depending on the area of an absorber $g = f(A_{ab})$.

Regime $g \neq f(A_{ab})$ means that the heat-transfer agent charge is set for one, base, area PVT and with area change its value remains to constants. In the given work in the capacity of the base the charge of a fluid typical for solar solar collector is accepted g = 0.015 l/s per 1 m^2 the absorber area. Thus, alternative sizes of the channel, proceeding from the accepted conditions on fixing of settlement width (1 m). Will be defined by length of the channel.

On average temperature of an absorber ($\overline{t}_{ab}$) the ambient air temperature influences (fig. 2) at increase t_a it grows. However rate of change ($\overline{t}_{ab}$) depends on length of the channel. With increase in length rate increases. From this it follows that at change of external conditions low temperatures of an absorber are characteristic for collecting panels of small sizes. The data is resulted for one value of intensity of solar intensivity – 800 W/m^2, but similar dependence occurs and at other values of irradiance.

As absorber and heat-transfer agent temperatures are interconnected, for generalisation of the solution of system of the equations we introduce a complex defining a relationship of change of temperature of heat-transfer agent and average temperature of an absorber. Such complex we name efficiency ratio of a heat transport from an absorber to chilling heat-transfer agent and we express in an aspect:

$$\eta_{he} = \frac{\delta t_f}{\bar{t}_{ab}} \tag{5}$$

where:

$\delta t_f = t''_f - t'_f$;

t'_f and t''_f – inlet and outlet temperatures of heat-transfer agent.

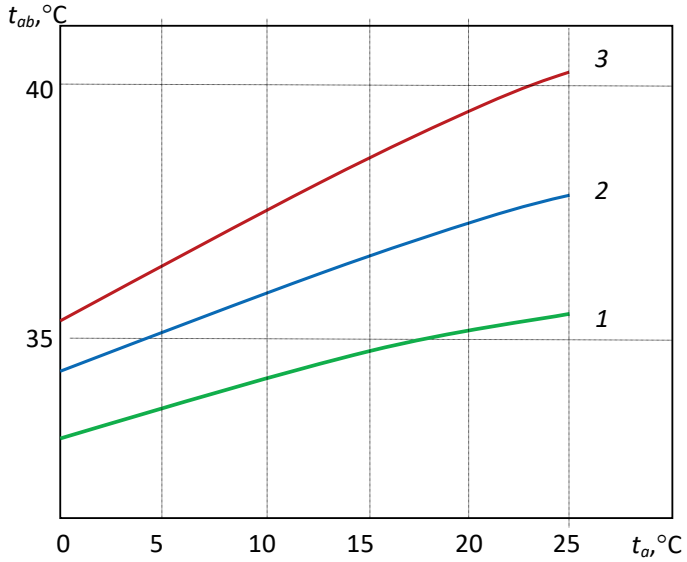

FIGURE 2. *Influence of amdient temperature and length of the channel on average temperature of an absorber at the constant charge of a fluid. Length of the channel: 1 – 1 m; 2 – 1.5 m; 3 – 2.0 m*

For PVT a concrete design the heat transport efficiency ratio depends on external conditions: ambient temperature and intensity of insolation (fig. 3). With increase in these parameters η_{he} increases. Besides, the additional factor of dependence is the length of the channel. The increase in length raises influence of these parametres on function. Thus, value η_{he} cannot be to the accepted constants and at regime calculations it is necessary to consider affecting of conditions of realisation of process.

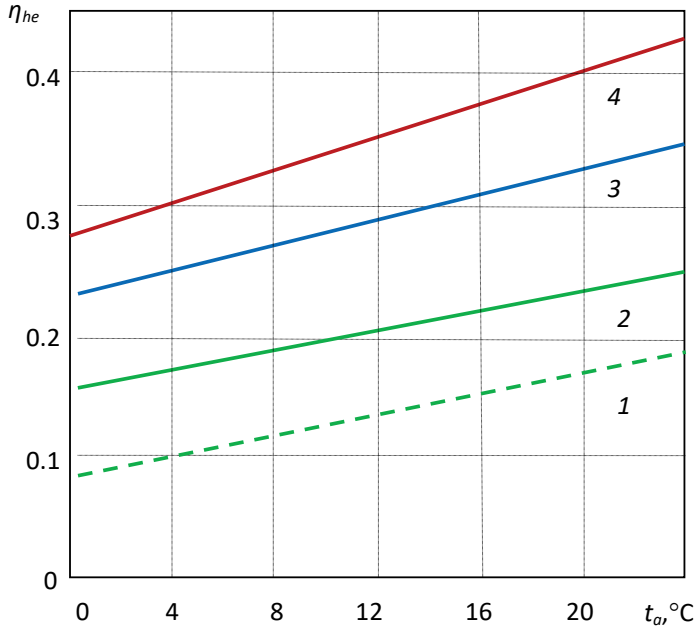

FIGURE 3. *Influence of external conditions on heat transport efficiency ratio at the constant charge of a flued. Length of the channel, intensity of radiation: 1 – 1 m, 500 W/m²; 2 – 1 m, 800 W/m²; 3 – 1.5 m, 800 W/m²; 4 – 2.0 m, 800 W/m²*

As showed the analysis, the greatest influence on heat transport efficiency ratio under constant hydraulic conditions is rendered by intensity of radiation, temperature of ambient air and absorber area. Taking into account it generalising dependence in an aspect is gained:

$$\eta_{he} = 0.1\left[t_a\left(\frac{A^*}{H}\right)^{0.48} - 1\right] + \left(0.424A^* - 0.0253\right)\exp\left(-\frac{233A^* + 141}{H}\right) \quad (6)$$

where:

H – intensity of radiation;

t_a – ambient temperature;

A^* – the area of an absorber led to its width.

Offered dependence can be used for definition of temperature of an absorber and outlet temperature of heat-transfer agent of the combined solar device in problems of regime optimisation. As characteristic temperatures – components of efficiency ratio of a heat transport are interconnected and defined by concrete conditions, for a finding of one of them from definition of a complex for η_{he} it is necessary to have a well-founded method of calculation another. Taking into account it, on the basis of resulted above model, dependence for average temperature of an absorber has been gained:

$$\overline{t}_{ab} = 1.306(14.6 - A^*) + 0.00464 \cdot H(3.22 + A^*) + 0.0667 \cdot t_a \quad (7)$$

This dependence at the found value of efficiency ratio can be used for temperature drop definition in chilling heat-transfer agent and a outlet reheat temperature t''_f at the accepted reference temperature. Here in the capacity of the initial accepts temperature 20°C.

In a regime $g = f\left(A_{ab}\right)$ the fluid consumption variable, proportionally depending on the absorber area. Under such circumstances the absorber temperature does not depend on its sizes. On figure 4 characteristic dependence between temperature of an absorber and external temperature is shown. Parametre here is magnitude of irradiance. Growth of external temperature, and also intensity of irradiance leads to increase in temperature of an absorber. This dependence for all sizes of the channel matches to conditions of base alternative with the area 1 m² (length, equal 1 m).

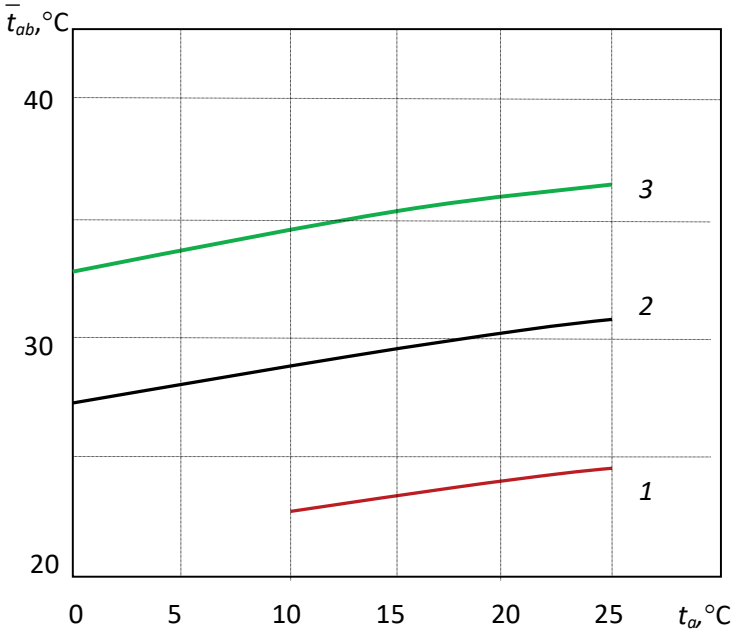

Figure 4. *Dependence of temperature of an absorber on ambient temperature and irradiance at the variable consumption of a fluid, W/m²: 1 – 200; 2 – 500; 3 – 800*

The efficiency ratio submits to the dependences, gained for base alternative, and its magnitude does not depend on absorber sizes. Thus, at any sizes PVT of the deepest cooling it is possible to achieve in a regime $g = f\left(A_{ab}\right)$.

Proceeding from the gained data, the greatest influence on heat transport efficiency ratio under constant regime conditions is rendered by intensity of radiation and ambient temperature. Taking into account it for a refrigerating duty $g = f\left(A_{ab}\right)$ generalising dependence in an aspect is gained:

$$\eta_{he} = 0.143 \cdot \ln(H) - 0.797 + t_a (119 + 0.194H)^{-1} \tag{8}$$

Conclusions

Features of temperature refrigerating duties of hybrid solar collector are shown. For generalisation of the solution of system of the equations the temperature factor is introduced η_{he}. Which defines a relationship of change of temperature of heat-transfer agent and average temperature of an absorber and is a parametre of efficiency of a heat transport from an absorber to chilling heat-transfer agent. The greatest agency on heat transport efficiency ratio under constant hydraulic refrigerating conditions is rendered by intensity of radiation, ambient temperature of air and absorber area. At the heat-transfer agent charge, connected with the absorber area, its magnitude does not render agency on transfer efficiency ratio. Generalising dependences for calculation of temperature characteristics are offered. Offered dependences can be used for definition of temperature of an absorber and outlet temperature of heat-transfer agent of the hybrid solar device in problems of regime optimisation. Any of these parametres can be set any way.

References

[1] Barbu M., Darie G., Siroux M., *A Parametric Study of a Hybrid Photovoltaic Thermal (PVT) System Coupled with a Domestic Hot Water (DHW) Storage Tank*, Energies, 2020, 13, 6481.

[2] Sevela P., Olesen B., *Gibridny solnechny kollektor*, Zdanija Vysokih Tehnology, 2013, No. 2, pp. 90-97.

[3] Harchenko V.V., Nikitin B.A., Tihonov P.V., Makarov A.E., *Teplosnabgenje s icpolzovaniem fotoelekticheskih moduley*, Tehnika v Selskom Hozjaystve, 2013, No. 5, pp. 11, 12.

[4] Sabirzjanov T.G., Kubkin M.V., Soldatenko V.P., *Matematicheskaja model fotobatarey kak istochnika elektricheskoy energii,* Tehnika v Selskogospodapskom Vyrobnictvi, 2012, Vyp. 25, Ch. 1, pp. 331-335.

Boris BASOK, Boris DAVYDENKO[1]
Anatoliy PAVLENKO[2]

[1] *Institute of Engineering Thermophysics of the National Academy of Sciences of Ukraine*
[2] *Kielce University of Technology, Poland*

DOI: 10.53412/jntes-2021-3-3

GENERATION OF PRESSURE OSCILLATIONS IN AIR FLOWS IN VERTICAL CHANNELS WITH INTERNAL HEAT RELEASE

Abstract: *The characteristics of the air flow in a vertical channel, arising due to local internal heat release, are investigated by the method of numerical simulation. Heat is supplied to the flow from internal sources located in a limited volume closer to the inlet section of the channel. The problem of flow and heat transfer is described by a system of unsteady Navier-Stokes and energy equations for a compressible medium. The coefficients of viscosity and thermal conductivity are considered to be temperature dependent. From the numerical solution of this system, the velocity, pressure, and temperature fields in the channel are determined. Based on the results of the calculations, the regularities of the change in time of velocity and pressure in the channel are determined. From the analysis of the results it follows that from the moment the heat supply begins, a vertical air flow develops in the channel, which is accompanied by oscillations in velocity and pressure. Self-oscillations arising in a gas flow are a manifestation of instability of flow. It is shown that stable oscillations take place in the presence of additional local hydraulic resistance in the channel. The dependence of the amplitude and frequency of pressure oscillations and the air flow velocity on the power of the sources of internal heat release and the height of the channel has been investigated. It was determined that with an increase in the power of the source of internal heat supply and the height of the channel, the amplitudes of the velocity and pressure fluctuations increase.*

Keywords: *natural convection, numerical modeling, flow instability, pressure self-oscillations, oscillation amplitude.*

Introduction

Periodic self-oscillatory processes accompanying the supply of heat into the flow of a compressible medium is an important factor that must be taken into account when designing heat and power equipment. Thermoacoustic self-oscillations can occur when heat is supplied by convection to the flow from an external source or when fuel mixtures are burned in different thermal devices. Self-oscillations of pressure can create additional mechanical loads on the structure of the combustion device, which can lead to its damage. This regime can also change the heat transfer conditions. Therefore, an important problem is to determine the dependence of the characteristics of self-oscillations on the level of thermal load on the system, as well as on the geometric characteristics and operating parameters of the furnace devices.

Thermoacoustic self-oscillations arising in a gas flow is one of the manifestations of flow instability. An unstable flow regime occurs in the elements of power equipment, if there is an internal release of heat in a limited volume of it, or there is an external supply of heat. One of the well-known processes accompanied by the generation of thermoacoustic self-oscillations is vibrational combustion. This phenomenon is observed during the combustion of fuel mixtures in air heaters for blast furnaces, in the combustion chambers of jet engines and in a number of other devices. At certain frequencies and

amplitudes, such oscillations can become dangerous to equipment and can lead to its destruction. Self-oscillations of pressure do not allow increasing the power and economic performance of power equipment. The regularities of this phenomenon have not yet been sufficiently studied. Therefore, there are problems with the definition of ways to prevent its destructive action. It follows from this that the problem of the occurrence of pressure self-oscillations in the flow of coolants is urgent today.

The Rijke tube is often used as an object for studying thermoacoustic oscillations. Rijke tube is a channel with a located heat source. Acoustic oscillations are generated in such channel under certain conditions. The characteristics of these oscillations in the Rijke tube were investigated experimentally and theoretically on the basis of a number of mathematical models. A detailed review and analysis of the results of analytical and experimental studies related to the Rijke tube, carried out before 1993, is presented in [1]. The authors of [2] associate the relevance of research on self-oscillations in devices like the Rijke tube with problems arising in the combustion chambers of jet and rocket engines. Another problem, in connection with which the study of the Rijke phenomenon is relevant, is associated with processes in pulsed combustion chambers and coal bed combustors. In [3] a computational fluid dynamics technique is used to investigate the unsteady flow field inside a Rijke tube. This investigation is carried out to explain the coupling that exists in such environment between heat addition, pressure and velocity oscillations. It is shown that the location of the heat source is a key factor in producing oscillations inside the Rijke tube. It was found that pressure oscillations appear to grow exponentially with increasing of heat input.

Theoretical studies of thermoacoustic oscillations were carried out mainly at simplified mathematical formulations of problems of hydrodynamics and heat transfer, which make it possible to obtain their analytical solutions. In [4], on the basis of a simplified mathematical model, including one-dimensional equations for the transfer of mass, momentum and energy, an analysis of the characteristics of acoustic oscillations in a Rijke tube with internal heat supply from electrically heated grid is carried out. The mathematical model proposed in [4] for the Rijke tube is recommended to be used for preliminary design and analysis of real thermal devices, where thermoacoustic instability may occur. In [5], using a similar one-dimensional mathematical model, the thermoacoustic instability in the Rijke tube was investigated. By using the Galerkin approximation, a thermoacoustic model was built, on the basis of which the study of velocity and pressure perturbations was carried out. With the obtained research results, a control scheme for a combustion device similar to the Rijke tube has been developed.

In [6], the thermoacoustic instability in a Rijke tube with a distributed heat source is investigated by solving a system of one-dimensional equations of momentum and energy transfer. Due to the widespread of thermoacoustic instability in the combustion chambers of gas turbines, this work is aimed to study this phenomenon and to solve this problem. The heat release model consists of a number of distributed heat sources with individual heat release rates. This paper examines the influence of multiple heat sources, time delay of heat release on nonlinear system characteristics associated with a distributed heat source. It was found that a distributed heat source plays an important role in determining the stability of a thermoacoustic system.

The results of theoretical and experimental studies of thermoacoustic instability during combustion are presented in [7]. The work uses an approach to modeling based on a separate description of the hydrodynamic and acoustic fields. It is shown that this combined method is extremely effective, and the calculation results are confirmed by corresponding experiments.

In [8], the results of studies of pressure self-oscillations arising in combustion installations are presented. The theoretical research is based on the energy method. On its basis, a theoretical model has been developed that makes it possible to consider the self-excitation of longitudinal acoustic oscillations of a gas in typical combustion devices. In this case, it is believed that self-oscillations arise due to the presence of a phenomenological delay in the combustion process.

In [9] it is noted that pressure self-oscillations arise not only during combustion, but also during convective supply of heat into the flow. That is, in addition to the phenomenological delay in the combustion process, there are also other reasons for the excitation of self-oscillations, among which the

so-called “negative” viscous friction resistance. It manifests itself in the form of a decrease, under certain conditions, of the frictional resistance in the channel with an increase in the flow velocity. Due to the fact that the viscosity of air increases with increasing temperature, an increase in the flow rate, which is accompanied by a decrease in temperature, can lead to a decrease in frictional resistance. In [10], the mechanisms of thermohydraulic instability of a gas flow with a local supply of heat were determined. The corresponding mathematical model of gas movement has been built. For the model under consideration, the thermal energy dissipation tensor is determined, which characterizes the presence of negative resistance. A simplified method for calculating the parameters of self-oscillations arising from unstable vibrational combustion in vertical combustion chambers of blast furnace stoves is described in [11].

In [12], the regularities of the occurrence of thermoacoustic instability inside a horizontal Rijke tube are investigated by an experimental method. The Rijke tube is equipped with a coaxial burner with gas premixing as a heat source, which can be placed in any position inside the tube. Methods for suppressing this instability are considered.

A generalization of the results of analytical studies of pressure self-oscillations obtained by solving the system of equations of motion of a continuous medium are presented in [13].

Since the considered research results were obtained using simplified mathematical models that make it possible to obtain analytical solutions, these results mainly describe the conditions for the occurrence and the qualitative nature of self-oscillations. To determine the quantitative characteristics of self-oscillations, it is necessary to apply more precise formulations of the problems of hydrodynamics and heat transfer and numerical methods for their solution. This research is carried out in order to determine the regularities of the occurrence of pressure self-oscillations in the flow of a compressible medium during local heat supply.

Materials and methods

To determine the characteristics of self-oscillations of pressure in the flow of a compressible medium, numerical modeling of the dynamics of air flow and energy transfer in a vertical channel with local internal supply of heat to the flow is performed. Air flow occurs due to natural convection arising from the internal local supply of heat to the air medium. Heat is supplied over a certain section of limited length Δz due to the action of internal sources. This section is located closer to the inlet cross section of the channel.

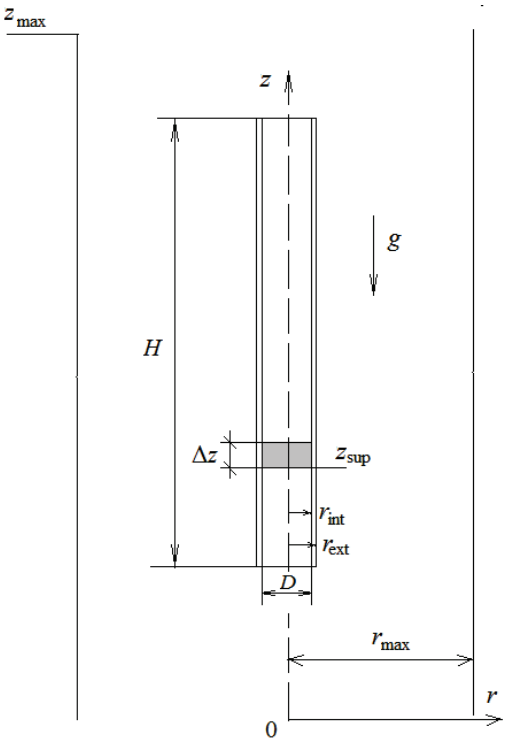

FIGURE 1. *Scheme of computational domain*

Numerical studies of hydrodynamics and heat transfer in a vertical channel, as well as an analysis of the possibility of thermohydraulic instability in the flow, are carried out in the computational domain (fig. 1), which includes a cylindrical channel, which is located in a cylindrical cavity with open upper and lower sections. Cavity radius – $r_{\max}$, cavity height – $z_{\max}$.

The movement of the compressible air medium in a cylindrical vertical channel is considered symmetrical about the axis of the cylinder. This motion is described by the system of Navier-Stokes and energy equations, which in polar coordinates has the form:

$$\frac{\partial \rho}{\partial \tau}+\frac{1}{r}\frac{\partial\left(\rho r v_r\right)}{\partial r}+\frac{\partial\left(\rho v_z\right)}{\partial z}=0 \tag{1}$$

$$\begin{aligned}\frac{\partial\left(\rho v_z\right)}{\partial \tau}+\frac{1}{r}\frac{\partial\left(\rho r v_r v_z\right)}{\partial r}+\frac{\partial\left(\rho {v_z}^2\right)}{\partial z}=-\frac{\partial p}{\partial z}+\frac{1}{r}\frac{\partial}{\partial r}\left(r\mu\left(\frac{\partial v_z}{\partial r}+\frac{\partial v_r}{\partial z}\right)\right)+\\ +\frac{\partial}{\partial z}\left(2\mu\frac{\partial v_z}{\partial z}-\frac{2\mu}{3}\left(\frac{1}{r}\frac{\partial\left(r v_r\right)}{\partial r}+\frac{\partial v_z}{\partial z}\right)\right)-\rho g\end{aligned} \tag{2}$$

$$\begin{aligned}\frac{\partial\left(\rho v_r\right)}{\partial \tau}+\frac{1}{r}\frac{\partial\left(\rho r {v_r}^2\right)}{\partial r}+\frac{\partial\left(\rho v_r v_z\right)}{\partial z}=-\frac{\partial p}{\partial r}+\frac{1}{r}\frac{\partial}{\partial r}\left(r\left(2\mu\frac{\partial v_r}{\partial r}-\frac{2\mu}{3}\left(\frac{1}{r}\frac{\partial\left(r v_r\right)}{\partial r}+\frac{\partial v_z}{\partial z}\right)\right)\right)-\\ -\frac{1}{r}\left(2\mu\frac{v_r}{r}-\frac{2\mu}{3}\left(\frac{1}{r}\frac{\partial\left(r v_r\right)}{\partial r}+\frac{\partial v_z}{\partial z}\right)\right)+\frac{\partial}{\partial z}\left(\mu\left(\frac{\partial v_z}{\partial r}+\frac{\partial v_r}{\partial z}\right)\right)\end{aligned} \tag{3}$$

$$\frac{\partial\left(C_p\rho T\right)}{\partial \tau}+\frac{1}{r}\frac{\partial\left(r C_p \rho v_r T\right)}{\partial r}+\frac{\partial\left(C_p \rho v_z T\right)}{\partial z}=\frac{1}{r}\frac{\partial}{\partial r}\left(r\lambda\frac{\partial T}{\partial r}\right)+\frac{\partial}{\partial z}\left(\lambda\frac{\partial T}{\partial z}\right)+q_v \tag{4}$$

$$p=\rho R_a T \tag{5}$$

where:

τ – time;
r – radial coordinate;
z – vertical coordinate;
v_r – radial velocity;
v_z – vertical velocity;
p – pressure;
g – acceleration of gravity;
T – temperature,
C_p – heat capacity of the gas at constant pressure;
ρ – air density;
μ – dynamic coefficient of air viscosity;
λ – coefficient of thermal conductivity of air;
q_v – density of internal sources of heat;
R_a – gas constant for air.

Dynamic viscosity coefficient μ (T) and thermal conductivity of air λ (T) depend on temperature.

Boundary conditions are formulated for this system. It is considered that at $z = 0$ the temperature and pressure of the gas are known. It is also assumed that the radial velocity component in the lower section of the computational domain is zero. At the exit from the computational domain $z = z_{\max}$, the pressure is also known. The radial velocity component at $z = z_{\max}$ is taken to be zero. It is also assumed that at $z = z_{\max}$ the derivative of the temperature along the z coordinate is equal to zero. So, the boundary conditions for the system of equations (1)-(5) are formulated as:

$$z = 0: p = p_0;\ v_r = 0;\ T = T_\infty \tag{6}$$

$$z = z_{\max}: p = p_{\text{ex}};\ v_r = 0;\ \frac{\partial T}{\partial z} = 0 \tag{7}$$

The air pressure at the outlet from the computational domain p_{ex} is determined from the expression:

$$p_{ex} = p_0 \cdot \exp\left(-\frac{g}{R_a T_\infty} z_{\max}\right) \tag{8}$$

which follows from the condition of equality between the pressure drop between the lower and upper cross sections of the computational domain and the weight of the air column located between these sections.

On the axis of symmetry $r = 0$, as well as on the boundary of the computational domain $r = r_{\max}$, the following boundary conditions are accepted:

$$r = r_0;\ r = r_{\max}: v_r = 0;\ \frac{\partial v_z}{\partial r} = 0;\ \frac{\partial T}{\partial r} = 0 \tag{9}$$

On the channel surfaces, the following conditions are accepted:

$$r = r_{\text{int}};\ r = r_{\text{ext}}: v_r = 0;\ v_z = 0;\ \frac{\partial T}{\partial r} = 0 \tag{10}$$

The system of equations (1)-(5) with boundary conditions (6)-(10) is solved by the finite difference method. For this, a computational grid is constructed and the approximation of partial differential equations by finite differences is performed according to the scheme given in [14]. The system of finite difference equations is solved by the matrix method [15]. Based on the results of its solution, the fields of velocity, pressure and temperature are determined, which change in time.

Results

In figure 2 shows the velocity and temperature fields in a vertical channel with a height H =1.1 m and a diameter D = 0.1 m, obtained for the case of heat supply with a power Q = 3000 W from an internal volumetric source. The beginning of the heat supply section is at a distance of 0.16 m from the inlet cross section of the channel. The length of this section is 0.13 m. The results are given for three moments of time. It is assumed that at $z = 0$ the air temperature is T_∞ = 293 K, and the pressure is p_0 = 101000 Pa.

In figure 3 shows the changes in time of the air flow velocity in the inlet (fig. 3a) and in the outlet (fig. 3b) sections of the channel at a time interval of 1.45 s < τ < 1.50 s. As can be seen from this figure, the time variation of the velocity in these cross sections has the character of oscillations with variable amplitude. The average velocity in the inlet section reaches 1.04 m/s, and in the outlet section – 2.05 m/s. That is, the average velocity at the exit from the channel is twice the flow velocity at the entrance to the channel. The frequency of velocity oscillations is $\omega_v \sim 240$ Hz.

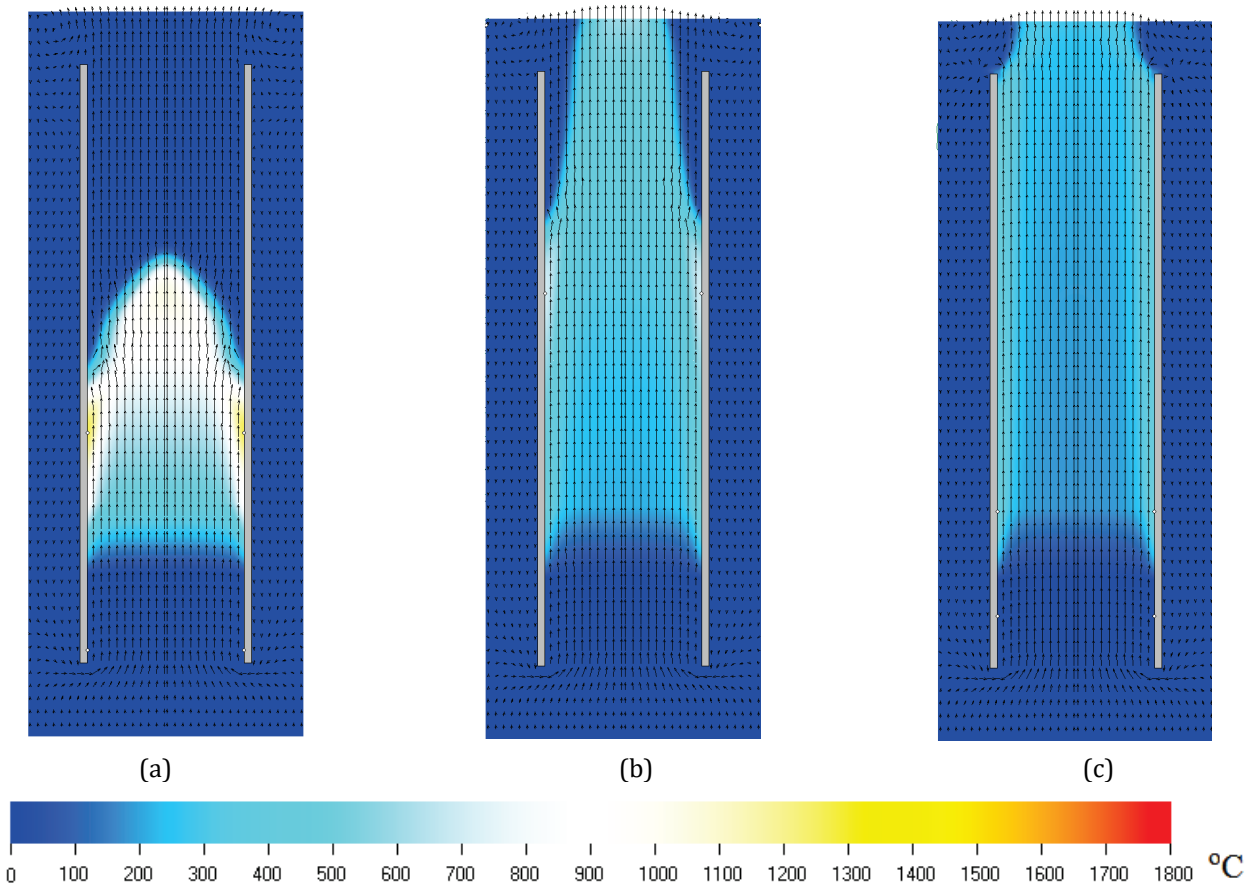

FIGURE 2. *Velocity and temperature fields in the vertical channel under the conditions of heat supply with power Q = 3000 W: a) τ = 1.0 s; b) τ = 1.5 s; c) τ = 2.0 s*

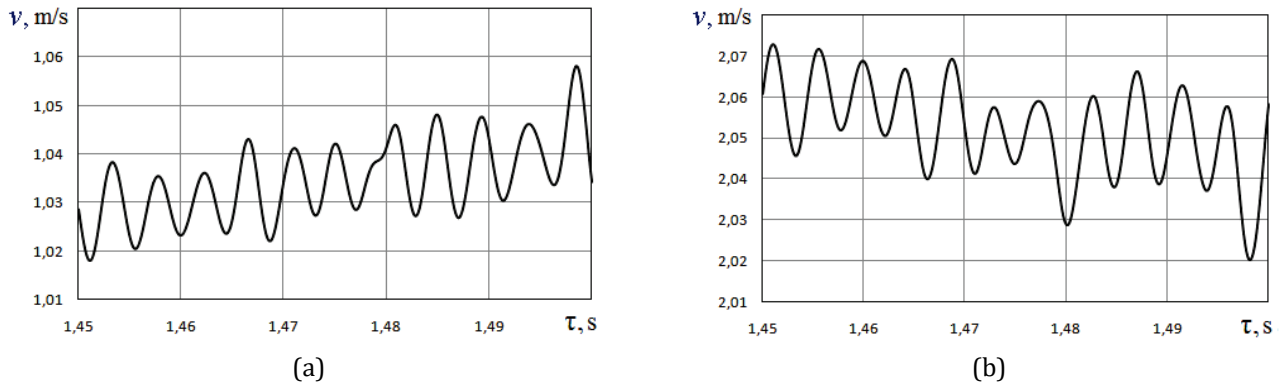

(a) (b)

FIGURE 3. *Change of flow velocity in the inlet (a) and outlet (b) cross sections of the channel in the time interval 1.45 s < τ < 1.50 s under the conditions of heat supply with power Q = 3000 W*

A characteristic feature of the oscillatory motion of the gaseous medium in a vertical channel with a local heat supply is that the oscillations of the velocity at the exit from the channel are in antiphase with the oscillations of the velocity at the entrance to the channel. That is, at the maximum flow velocity at the outlet from the channel, the flow velocity at the inlet to the channel will be minimal, and at the minimum flow velocity at the outlet from the channel, the inlet velocity will be maximum. This can be seen from a comparison of the graphs shown in figure 3a and figure 3b. This indicates that the gas flow, moving upward under the action of the thermogravitational force, simultaneously performs oscillatory motion, expanding and narrowing in the direction of the inlet and outlet cross sections of the channel.

The time variation of the excess pressure in the channel cross section, which is located at a distance of 0.1 m from the outlet cross section, in the time interval 1.45 s < τ < 1.50 s are shown in figure 4. The excess pressure is measured from its value at z = 0, where it is equal to p_0. As can be seen from this figure, the time variation of the pressure in this section has the character of oscillations occurring with variable amplitude (from 1.5 Pa to 2 Pa) and with a frequency of $\omega_p \sim$ 240 Hz (with the same frequency as the velocity oscillations).

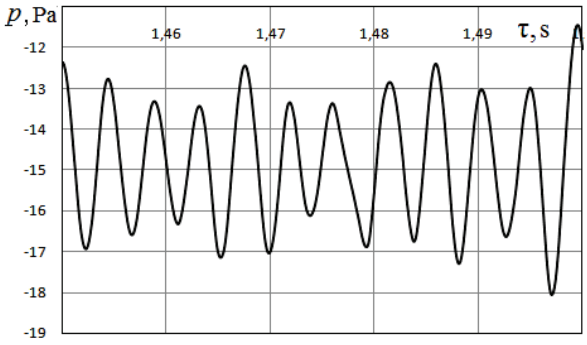

FIGURE 4. *Change of excess pressure in the cross section, located at a distance of 0.1 m from the outlet cross section of the channel, in the time interval of 1.45 s < τ < 1.50 s under the conditions of heat supply with power Q = 3000 W*

As follows from the results of calculations, the amplitudes of the velocity and pressure oscillations in the channel under the considered conditions decrease with time. After a while, the oscillations practically damp out due to dissipative effects.

In devices in which the combustion process of the fuel mixture (combustion chambers) takes place, there are usually separate elements that create additional local hydraulic resistance to the gas flow. Such elements can be, for example, flame stabilizers. Schematically, they can be represented as a system of concentric rings located in the channel and having a common axis of symmetry with the channel. The results of calculating the velocity and temperature fields under the same conditions that were considered earlier for a channel with a system of concentric rings near the outlet section of the channel are shown in figure 5. As can be seen from the comparison of figure 2 and figure 5, in the presence of these cylindrical rings, the velocity and temperature fields in the channel develop in time somewhat differently than in the absence of additional hydraulic resistance.

In figure 6 shows the time variation of the excess pressure in the channel section, located at a distance of 0.1 m from its outlet section. The results are compared for channels without local hydraulic resistance (1) and with local hydraulic resistance (2). The local heat release power is Q = 3000 W. From a comparison of the results presented in figure 6, it follows that in the time interval 1.0 s < τ < 1.05 s (fig. 6a), pressure oscillations occur both in the channel without local hydraulic resistance (1) and in the channel with local hydraulic resistance (2). But at τ > 2 s, pressure oscillations in the channel without local hydraulic resistance almost stop (fig. 6b, curve 1), while in the channel with local hydraulic resistance, pressure oscillations continue with a variable amplitude of ~3.0 Pa, ..., 3.5 Pa and with a frequency of ~240 Hz.

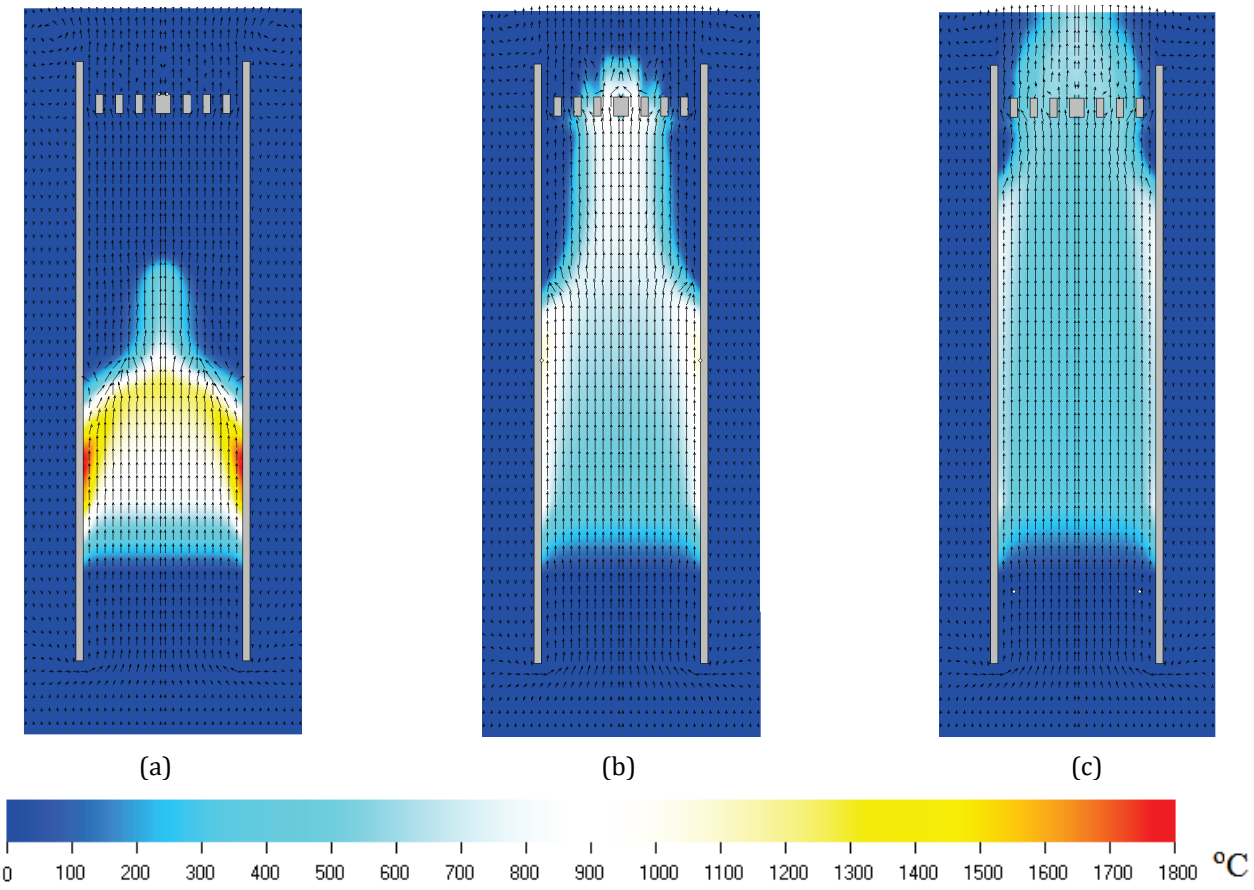

FIGURE 5. *Velocity and temperature fields in a vertical channel with local hydraulic resistance under conditions of heat supply with power Q = 3000 W: a) τ = 1.0 s; b) τ = 1.5 s; c) τ = 2.0 s*

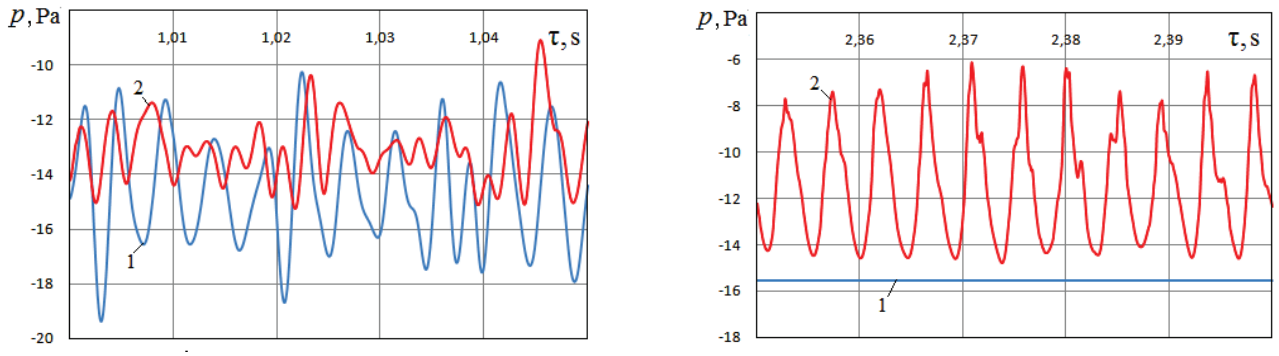

FIGURE 6. *Change in time of excess pressure in the cross section, located at a distance of 0.1 m from the outlet cross section of the channels with height H = 1.1 m without local hydraulic resistance (1) and with local hydraulic resistance (2) with local heat supply Q = 3000 W: a) 1.0 s < τ < 1.05 c; b) 2.35 s < τ < 2.4 s*

To determine the influence of the power of internal sources of heat release on the amplitude of pressure oscillations in a vertical channel with a height of H = 1.1 m with a local heat supply, the problem considered is solved also for Q = 2000 W and Q = 1000 W. The change in time of the excess pressure in the section, located at a distance of 0.07 m after the source of heat release (a) and in the section, which is located at a distance of 0.1 m from the outlet section of the channel (b) at three values of the power of the heat release source (Q = 3000 W; Q = 2000 W and Q = 1000 W) are shown in figure 7. The considered time interval is 6.215 s < τ < 6.25 s. As can be seen from this figure, with a decrease in the power of the heat release source, the amplitude of pressure oscillations also decreases in both cross sections of the channel. That is, an increase in the power of the heat source leads to an increase in the amplitude of pressure oscillations.

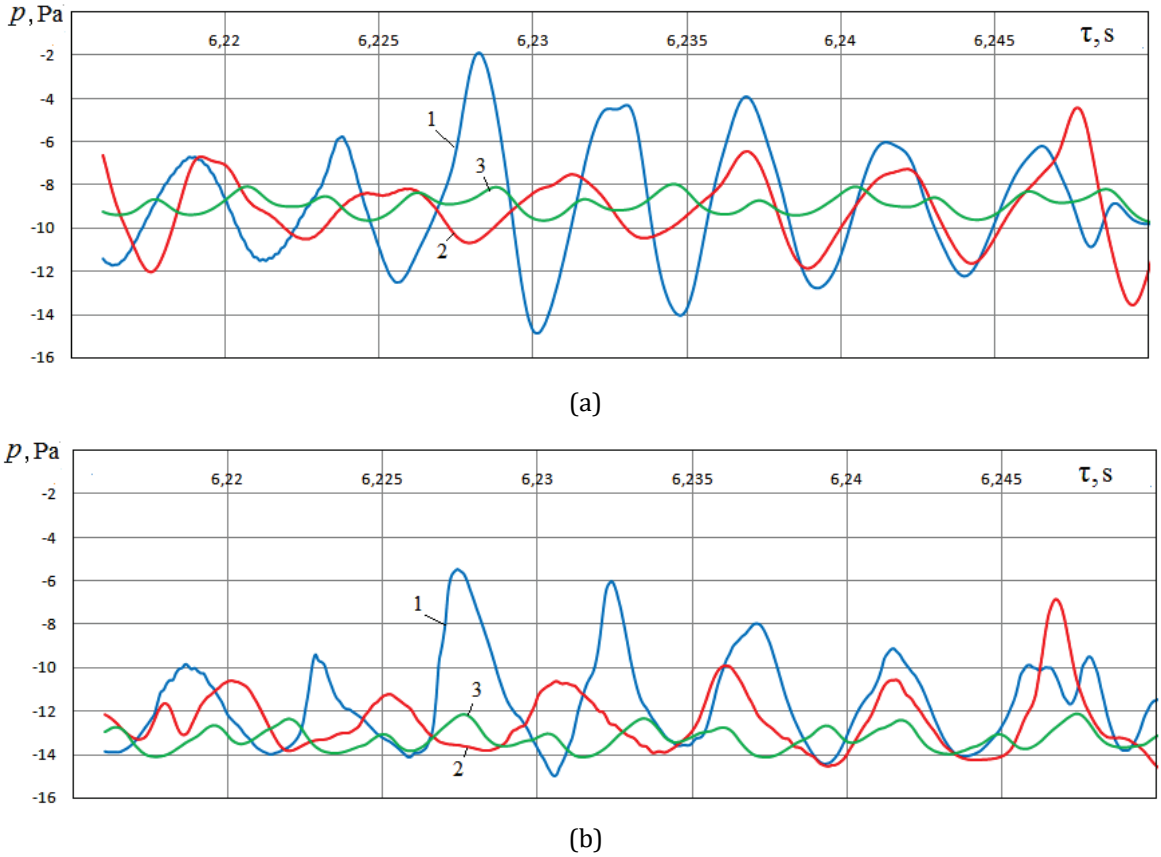

FIGURE 7. *The change in time of the excess pressure in the cross section located at a distance of 0.07 m after the source of heat release (a) and in the section, located at a distance of 0.1 m (b) from the outlet section of the channel at different power of heat release: 1 – Q = 3000 W; 2 – 2000 W; 3 – 1000 W*

The influence of the power of internal sources of heat release on the time variation of the flow velocity in the inlet and outlet sections of the channel with height H = 1.1 m and diameter D = 0.1 m with local hydraulic resistance is shown in figure 8. As in figure 7, cases of three values of the power of sources of heat release are considered: Q = 3000 W; Q = 2000 W and Q = 1000 W. As can be seen from the figure, the average velocities in the inlet section of the channel are: 0.595 m/s at Q = 3000 W; 0.65 m/s at Q = 2000 W and 0.635 m/s at Q = 1000 W. In the outlet section of the channel, the velocities are: 1.35 m/s at Q = 3000 W; 1.19 m/s at Q = 2000 W and 0.92 m/s at Q = 1000 W. It follows from this that with an increase in the power of internal sources of heat release, the velocities in the outlet section of the channel increase. For the inlet section of the channel, such a pattern is not observed. Figure 8 also shows that the amplitudes of the velocity oscillations increase with the increase in the power of the heat generation sources.

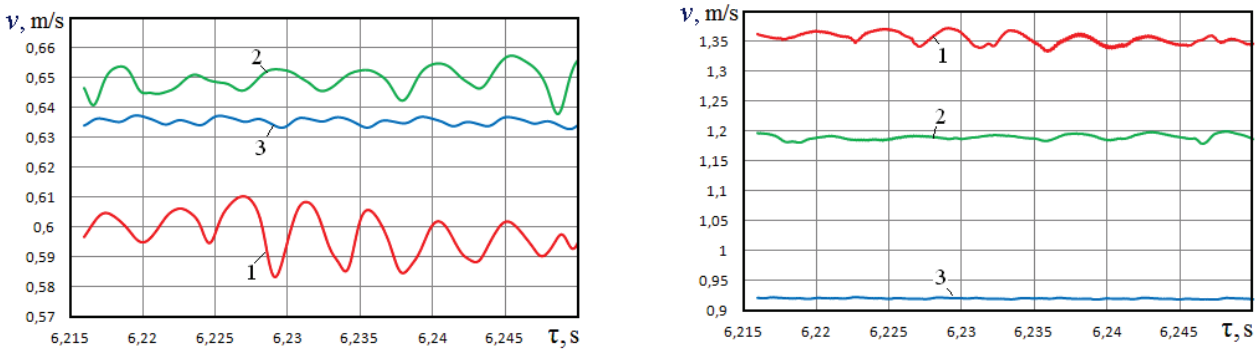

FIGURE 8. *Change in velocity over time in the input (a) and output (b) cross sections of the channel at different capacities of local heat sources: 1 – Q = 3000 W; 2 – 2000 W; 3 – 1000 W*

To determine the influence of the channel height on the characteristics of self-oscillations of pressure in the air flow, the problem was solved also for H = 2.0 m at Q = 3000 W. Other initial data for this case are the same as for H = 1.1 m. Based on the results of numerical modeling, the flow characteristics in channels of different heights are compared. Comparison of the nature of the change in time of excess pressure in the cross-sections of the channels that are located at a distance of 0.3 m from their inlet cross-sections, and in the cross-sections that are at a distance of 0.1 m from the outlet cross-sections of the channels are shown in figure 9. As can be seen from this figure, with the same power of heat generation sources, the amplitude and frequency of pressure oscillations at the same time intervals (6.41 s < τ < 6.44 s) will be different for channels of different heights. With an increase in the total height of the channel H and the same powers of the heat generation source, the amplitude of pressure oscillations in the above-mentioned sections of the channels increases. At the same time, the frequency of these oscillations decreases with increasing channel height. At H = 1.1 m, the frequency is $\omega_p \sim 240$ Hz, and at H = 2.0 m, it is $\omega_p \sim 135$ Hz.

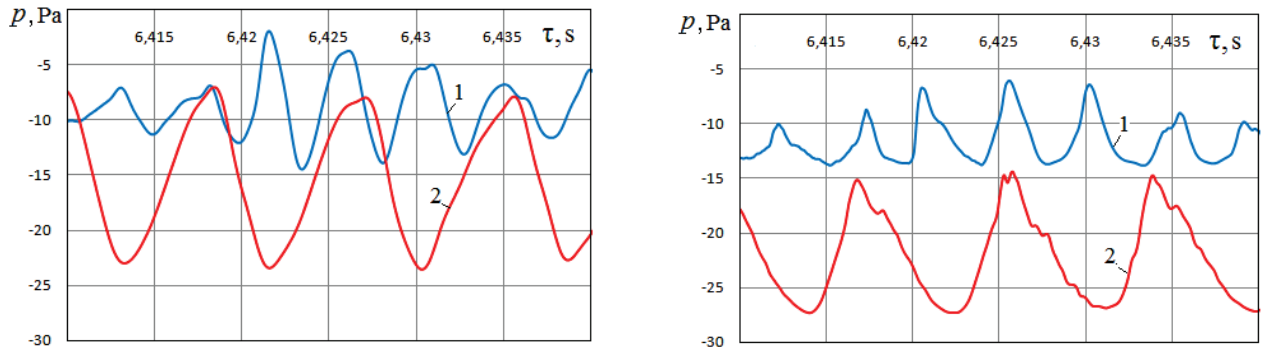

FIGURE 9. *Change in time of excess pressure in the cross sections of the channels located at a distance of 0.3 m from the inlet sections (a) and in the sections located at a distance of 0.1 m (b) from the outlet sections at Q = 3000 W: 1– H = 1.1 m; 2 – H = 2.0 m*

The time variation of the flow velocities in the inlet and outlet sections of channels with a height of H = 1.1 m and H = 2.0 m at local heat sources power Q = 3000 W is shown in figure 10. As can be seen from the figure, the flow velocity, as well as the amplitude and frequency of velocity oscillations at the same time intervals (6.41 s < τ < 6.44 s) will be different for channels of different heights. With an increase in the height of the channel H, the average velocity also increases both in the inlet and in the outlet sections of the channel. This is due to the fact that as the height of the channel increases, the difference between the external pressure drop and the weight of the air in the channel grows. The amplitude of the velocity oscillations in the inlet and outlet sections of the channel increases with increasing channel height H, and the frequency of the velocity fluctuations decreases, as does the frequency of pressure oscillations.

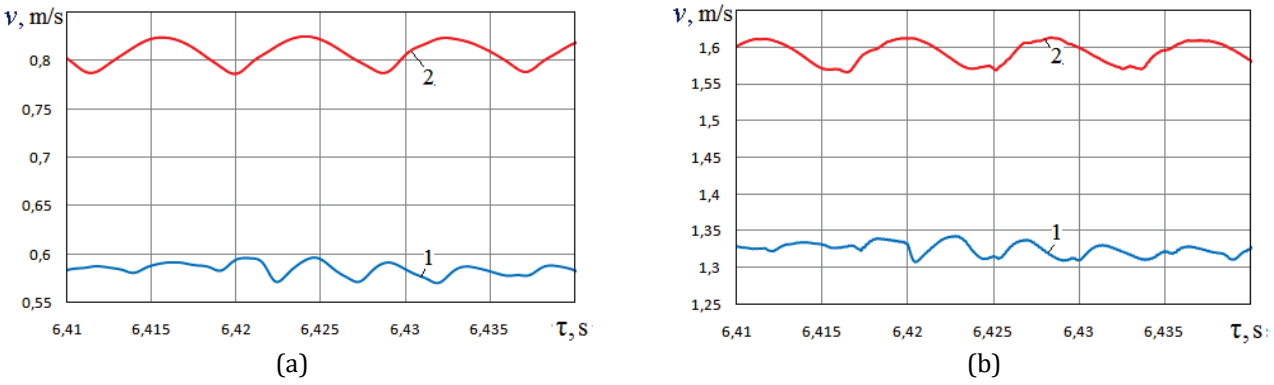

FIGURE 10. *Change in velocity over time in the input (a) and output (b) cross-sections of the channel with local hydraulic resistance at the power of heat sources Q = 3000 W: 1– H = 1.1 m; 2 – H = 2.0 m*

Conclusions

With a local internal supply of heat to a compressible gaseous medium, which is located in a vertical channel, self-oscillations of pressure and velocity arise. Self-oscillations arising in a gas flow are one of the manifestations of flow instability. In the section of the channel, where the internal release of heat occurs, with the increase in temperature, the velocity of the free convection air flow in the channel also increases. The value of the velocity in the inlet section is always less than in the outlet section. Velocity oscillations in the inlet and outlet sections of the channel occur in antiphase, that is, at the minimum velocity in the inlet section of the channel, the velocity in the outlet section will be maximum.

Self-oscillations of pressure and velocity in a vertical channel with local heat release tend to decay with time. Self-oscillations do not damp and are maintained for a long time at a certain level in the presence of additional local hydraulic resistance in the channel. The nature of pressure self-oscillations is inharmonious with a non-constant amplitude.

The amplitude of pressure and velocity self-oscillations in a channel with local internal heat release increases with an increase in the power of heat release sources, as well as with an increase in the height of the channel. The oscillation frequency decreases with increasing channel height.

References

[1] Raun R.L., Beckstead M.W., Finlinson J.C., Brooks K.P., *A review of Rijke tubes, Rijke burners and related devices,* Progress in Energy and Combustion Science, 1993, Vol. 19, pp. 313-364.

[2] Shekhar M., Sarpotdar N., Ananthkrishnan, Sharma S.D., *The Rijke Tube – A Thermo-Acoustic Device*, Resonance, January 2003, pp. 59-71.

[3] Entezam B., Van Moorhem W.K., *Modeling of a Rijke – tube pulse combustor using computational fluid dynamics*, American Institute of Aeronautics and Astronautics, 1997, Seattle, p. 15.

[4] Matveev K.I., *Thermo-acoustic instabilities in the Rijke tube: experiments and modeling,* Ph.D. Thesis, Institute of Technology, California 2003, p. 161.

[5] Molina Sandoval M.O., *Nonlinear control of a thermoacoustic system with multiple heat sources and actuators,* Dissertations and Theses, 2016, p. 62.

[6] Xiaochuan Y., Ali T., Shenghui L., *Thermoacoustic instability in a Rijke tube with a distributed heat source*, Hindawi Publishing Corporation, Journal of Thermodynamics, 2015, p. 9.

[7] Moeck J.P., *Analysis, modeling and control of thermoacoustic instabilities*, Technischen Universitat Berlin, 2010, p. 220.

[8] Larinov V.M., Zaripov R.G., *Avtokolebaniya gaza v ustanovkakh s goreniya,* Izdatelsnvo Kazanskogo Gos. Tekhn. Unsversiteta, Kazan 2003, p. 227.

[9] Basok B.I., Davydenko B.V., Gotsulenko V.V., *Avtokolebaniya v trube Riyke pri raspolozhenii elektro-nagrevatelya neposredstvenno na yeye vkhode*, Sibirskiy Zhurnal Industrial'noy Matematiki, 2013, 14, 2 (54), pp. 50-61.

[10] Basok B.I., Gotsulenko V.V., *Mekhanizmy teplogidrodinamicheskoy neustoychivosti pri lokal'nom podvode teploty k gazu*, Dopovidi Natsyonal'noy Akademyy Nauk Ukrayiny, 2018, 3, pp. 69-79.

[11] Basok B.I., Gotsulenko V.V., *Raschet parametrov avtokolebaniy v vertikal'noy kamere goreniya vozdukhonagrevatelya domennoye pechi pri neustoychivom gorenii*, Teploenergetika, 2015, 1, pp. 59-64.

[12] Deshmukh Nilaj N., Sharma S.D., *Experiments on heat content inside a Rijke tube with suppression of thermo-acoustics instability*, International Journal of Spray and Combustion Dynamics, 2017, 9(2), pp. 85-101.

[13] Basok B.I., Gotsulenko V.V., *Termogidrodinamicheskaya neustoychivost' potoka teplonositelya*, Kiev 2015, p. 412.

[14] Peyret R., Teylor T.D., *Computational Methods for Fluid Flow*, Springer-Verlag, New York 1983, p. 358.

[15] Davydenko B.V., *Metod matrichnoy progonki dlya resheniya setochnykh uravneniy gidrodinamiki*, Vostochno-Yevropeyskiy Zhurnal Peredovykh Tekhnologiy, 2008, 5 (35), pp. 7-11.

Alexander SHAVOLKIN, Iryna SHVEDCHYKOVA,
Ruslan MARCHENCKO, Andrii PISOTSKII

Kyiv National University of Technologies and Design,
2 Nemyrovych-Danchenko Str., Kyiv, 01011, Ukraine

DOI: 10.53412/jntes-2021-3-4

INCREASING THE EFFICIENCY OF A HYBRID PHOTOELECTRIC SYSTEM OF A LOCAL OBJECT WITH A STORAGE BATTERY USING FORECAST

Abstract: *The implementation of a photovoltaic system with a storage battery to meet the needs of a local object and the ability to generate energy into the grid during peak hours is considered. The principles of implementation of the planned generation of energy into the grid during peak hours with a decrease in electricity consumption from the grid have been substantiated. In this case, the setting of the SB degree charge is carried out according to the forecast of the generation of the photovoltaic battery for the next day with a preliminary estimate of the generation power to the grid. The updated value of the generation power to the grid is determined according to the forecast data by the beginning of the morning peak, taking into account the actual generation power of the photovoltaic battery. Subsequently, at the intervals of discreteness of the forecast, the value of the generation power into the grid is corrected taking into account the actual generation power of the photovoltaic battery, the load and the degree of storage battery charge. The storage battery charge mode is set taking into account the forecast data at the end of the morning peak. The corresponding algorithm of the system functioning was developed. Simulation of energy processes in the system for a daily cycle of operation with an estimation of the cost of paying for electricity has been carried out. In this case, the archived weather data were used. It is shown that with the adopted system parameters, this solution allows providing the power generation to the grid in the evening peak of 19% to the load power, and in the morning peak up to 200%. Reducing the cost of payment consumed by a local object from the electricity grid is at one tariff rate in the summer period from 1.6 times to 14 times, in winter from 1.1 to 1.55.*

Keywords: *planned energy generation to grid, storage battery degree charge, photovoltaic battery generation forecast, multi-zone tariffication, simulation.*

Introduction

The disadvantage of photoelectric systems (PES) is the uneven generation of electrical energy. The largest generation of energy from a photoelectric battery (PV) occurs at noon hours. This creates the problem of ensuring a balance between consumption and generation in the power system as a whole, as well as at the level of local microgrids with distributed generation. The energy consumption of most local objects (LO) is a general nature with peak morning and evening loads. Excess energy for generation into the grid appears only during the hours of maximum solar activity. An urgent task is the use of energy storage devices, both at the level of the power system and local grids with PES. In this case, there is an opportunity to reduce daily consumption from the distribution grid (DG) and carry out the planned generation of energy in the DG only during peak hours, which will contribute to the balance in the power system. At the same time, additional investments in a storage device (storage battery (SB)) should pay off by reducing the cost of paying for the electricity consumed by the LO from the grid. This is possible when improving the energy management of PES using the forecast of the PV generation and the possibilities of multi-zone payment.

The relevance of the issue of consumption localizing at the place of generation in world practice is confirmed by the wide proposition on the electrical market of hybrid inverters (HI) connected to a DG [1, 2]. Inverters contain of whole complex of equipment for photovoltaic (PV) and storage batteries. It is used to reduce power consumption from the grid and to implement the uninterruptible power supply function. In this case, the SB energy is used when the PV energy is insufficient for the functioning of the LO load. A numbers of HI [1] has the function of generating surplus energy in the DG, which usually takes place during the hours of the greatest solar activity and a decrease in load. The possibilities of the Internet are practically not used to predict generation of PV and control the generation and redistribution of energy.

The use of a "multiconverter" in a PES with a SB and a supercapacitor is considered in [3] with regard to local microgrids. However, its use is considered as a distributed power unit in a multi-user system under the control of a centralized smart energy management system. A similar structure, but without a supercapacitor, is shown in [4], where the problem of combining several PVs into an autonomous system is solved when the grid is disconnected. Task of energy management and grid generation is not considered.

The use of a SB imposes a number of peculiarities on PES control when the SB charge level is more than 80%. It implies the use of power regulation of PV. In [5], an option is considered with switching off the PV while maintaining the state of charge of the SB within 75-80%. Great opportunities are provided by the use of the current regulator of PV and SB [6] without additional recharge cycles of the SB.

The issue of transferring the energy, stored in the SB during the hours of the night tariff and the excess energy of the PV during the daytime, for using during peak loads is considered in [5]. It makes possible to exclude energy consumption from the DG during peak tariff hours and in the most part of the daytime. At the same time, the use of PES to meet the needs of the LO with a load schedule tied to the PV generation based on the forecast is considered. The PV generation forecast provides wide opportunities for improving the control and redistribution of energy in PES. Resource [7] provides the possibility to directly predict the PV generation but with a discreteness of 1 hour and a certain error to the actual generation. The issues of increasing the accuracy of forecasting with decreasing discreteness in time are considered in [8].

In [9] the prediction of SB charge degree using forecast of PV generation to reduce consumption from the DG is considered regarding PES with SB to meet the need of LO's. Energy generation into the grid is not considered. Application the multifunctional inverter in PES with SB is shown in [10]. The principals of operation modes realization, including generation into grid with possibilities limitation of generation power and autonomous operation mode, are presented. However, the issues of planned generation, control of SB charge degree and using the forecast of PV generation in order to achieve concrete result, are not considered.

The effective mean for estimation of energy processes in PES in daily cycle of operation is simulation [11]. In this case, the wide opportunities to research the processes with estimation of the cost of electricity payment decreasing are appearing.

Therefore, additional study is required to ensure the planned for the day ahead, uniform in time generation of electricity into DG during peak hours (with the exclusion of generation at other times). In this case, it's necessary to ensure the maximum cost decreasing on the payment for electricity, consumed from the GD under condition that power, consumed by the load, does not depend on weather and the season of the year.

The aim of the article is improving the principles of control of PES with SB at implementation the functions of ensuring needs of LO with the possibilities of uniform predicted energy generation into the grid in peak hours.

The main tasks of this work:

- to study the possibilities of ensuring of LO needs with uniform energy generation into the grid in peak hours with planning on the forecast a day ahead;

- to develop the principles of control of PES energy consumption and the converter unit functioning in the varies operation modes;
- to develop the simulation model to research the energy processes in system in daily cycle with estimation of efficiency at different tariff plans.

Result of research

The structure of PES with SB on the base of multifunctional grid inverter with regulation of PV generation P_{PV} is made according to the principles, presented in [10].

In PES structure the SB realizes the key function in redistribution of energy, generated by PV and consumed by load from the grid. At the same time, it is possible to compensate for the consumption of the LO load during peak hours due to the accumulation of surplus energy of the PV or cheaper electricity from the DG at multi-zone billing or at time of use payment. Generation into DG during peak hours, when P_{PV} is low or absent, is possible only due to the SB energy. Duration of evening peak is 4 hour in winter [12] (October-April) – from 17.00 (18.00) to 21.00 (22.00), 3 hour in summer (May-September) – from 20.00 to 23.00. When the LO load is the same in any season of the year, the energy W_L consumed by LO during peak hours is higher in winter than in summer. With the same energy supplied by the SB in winter, it is possible to generate surplus electricity in the DG in summer. With the correct choice of the ratio of the rated PV power P_{PVR} and the energy capacity of the SB $W_{BR} = U_B C_B$ (U_B – voltage, C_B – SB capacity (Ah)), it is possible to provide generation into DG during the evening peak and in winter. And here the question is not about a simple increasing in W_{BR}, since the SB needs to be charged by the evening peak. This requires energy, and to reduce consumption costs, it is preferable to use the PV energy and not energy from the DG. An increase in W_{BR} will lead to an increase in the duration of the SB charge and it will not have time to charge.

Based on the data [13] for PV with P_{PVR} = 1 kW in condition of Kyiv. For clear day of July the general generation is $W_{PVC} \approx$ 6 kWh, average daily power is P_{PVAV} = 250 W, recalculated to daytime (8.00-20.00) average value is P_{PVAVD} = 500 W. The length of the time to ensure a full charge of the battery is long enough. Therefore, we limit the initial value of the degree of SB charge at the evening peak Q^*_{SE} = 95% ($Q^* = 100Q/Q_R$, Q_R is rated charge (capacity, Ah)). The final value is Q^*_{EE} = 50%, taking into account the acceptable value of the degree of discharge DOD = 50% (for lead-acid SB of the OPzV12-100 [14] type at about 3000 discharge cycles).

Energy W_{BL}, transferred by the SB to the load:

$$W_{BL} = 0.01\left(Q^*_{SE} - Q^*_{EE}\right)W_{BRL}$$

where $W_{BRL} = W_{BR} \cdot \eta_C \cdot \eta_B$, η_C and η_B are efficiency of converter unit and SB efficiency.

We have two deep SB discharge cycles per day in the presence of morning and evening load peaks. Let us introduce restrictions: for winter – $Q^*_{Sm} \geq 80\%$, $Q^*_{Em} \geq 60\%$ (morning peak), Q^*_{EE} = 50%; for summer – $Q^*_{Sm} \geq 80\%$, $Q^*_{Em} \geq 70\%$, Q^*_{EE} = 60%. Limitation $90\% \geq Q^*_{Sm} \geq 80\%$ is introduced to limit energy consumption for SB charging at night. Regarding to PES to meet the needs of the LO without generation into DG, the ratio $P_{PVR} : W_{BR}$ = 1 : 2.75 is proposed in [5]. The average value of the load power for the evening peak in summer is $P_{LPES} = W_{BL}/t_{PES}$ = 283.5 W at W_{BR} = 2750 Wh and $\eta_C = \eta_B$ = 94%. In winter, when t_{EPW} = 4 h, the value decreases P_{LPEW} = 273 W. In evening peak in winter the load is a little higher then in morning peak – we accept 1.1. We also accept the load in the morning P_{LPm} = 210 W, in the evening P_{LPEW} = 230 W with possibility of generation into DG in the evening P_{g2} = 40 W

($P^*_{g2} = 100P_{g2} / P_{LP} = 19\%$). In summer there is $P_{LPm} = P_{LPE}$ = 210 W with possibility of generation into DG in the evening P_{g2} = 70 W ($P^*_{g2} = 100P_{g2} / P_{LP} = 33.3\%$). At recalculation of PV power to P_{PVR} = 30 kW we will have: in winter P_{gw} = 1.2 kW, and energy W_{gw} = 4.8 kWh (at P_{LP} = 6.3 kW); in summer P_{gS} = 2.1 kW, and energy W_{gS} = 6.3 kWh. We accept, that average value of power of LO load is P_L = 210 W with a decrease of 15% (180 W) in the evening. Then, taking into account the fact that for summer P_{PVAVD} = 500 W, we obtain an overestimation of the PV power by 2.38 times.

In the morning peak (in summer from 8.00 to 11.00) the possibilities of generation increase since the PV energy is added (W_{PVPm} – according to the forecast data). The power P_{Lpm} value in this case:

$$P_{Lpm} = \frac{0.01\left(Q^*_{Sm} - Q^*_{Em}\right)W_{BRL} + W_{PVPm} \cdot \eta_C}{3} \quad (1)$$

Power generation P_{g1} into grid:

$$P_{g1} = P_{LPm} - P_{LP} \quad (2)$$

Diagram (fig. 1) illustrates W_{PVPm} changing depending on weather condition for May, July, September with values discreetness ΔW_{PVPm} = 100 Wh (by archive data [13] on 2015). The end value W_{PVm}, when the LO consumption without generation into grid is provided for values Q^*_{Sm} = 80%, Q^*_{Em} = 70%, P_{LP} = 210 W is W_{PVm0} = 411 Wh. At the same conditions and P_{g1} = 70 W there is value W_{PVm1} = 635 Wh. The end value W_{PVm}, when the LO consumption without generation into grid is provided for values Q^*_{Sm} = 90%, Q^*_{Em} = 70%, P_{LP} = 210 W is W_{PVm0} = 153 Wh. At the same conditions and P_{g1} = 70 W there is value W_{PVm1} = 376 Wh. When W_{PVm} = 1400 Wh there is value P_{g1} = 310 W (Q^*_{Sm} = 80%, Q^*_{Em} = 70%) and P_{g1} = 390 W (Q^*_{Sm} = 90%, Q^*_{Em} = 70%). Thus, in the period May-September the planned energy generation into the grid is realistic with a capacity of up to 1.86 and higher to the load power.

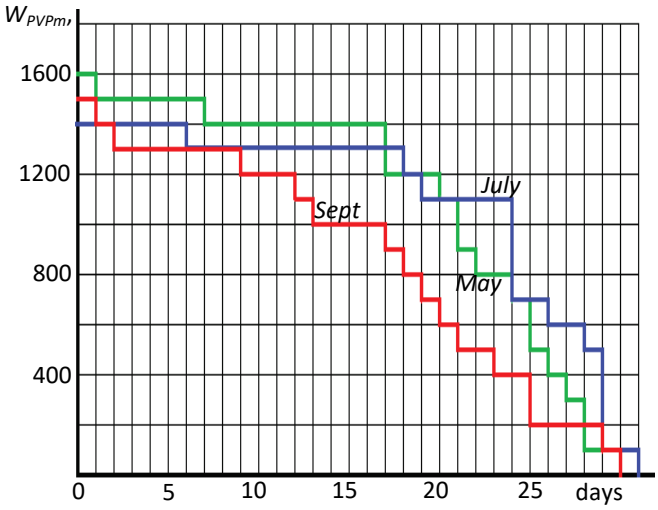

FIGURE 1. *Diagram of W_{PVPm}*

The daily cycle of PES operation were reviewed with reference to tariff zones [12] for summer season: t_1 = 7.00 – the end of night tariff zone; (t_2 = 8.00, t_3 = 11.00) – morning peak; t_4 = 16.00 – the end of the period of intensive solar radiation; (t_5 = 20.00, t_6 = 23.00) – evening peak; t_7 = 24.00 – the beginning of night tariff zone; (t_1, t_2), (t_3, t_5), (t_6, t_7) – daytime tariff zone. For winter: t_1 = 6.00, t_2 = 8.00, t_3 = 10.00,

t_4 = 14.30, t_5 = 17.00, t_6 = 20.00, t_7 = 23.00. After t_4 even in clear summer day PV energy is not enough to ensure the consumption of LO and the consumption of energy from the grid is inevitable. Charging SB characteristic of OPzV12-100 type [14] at $Q^* \geq 80\%$ is characterized by a decrease in charge current (table 1, where the average value I^*_{BAV} (in intervals 0.5 h) is presented in shares to $I_{BR} = 0.1\,C_B$ and relative power value on SB charge P_B to $P_{BR} = 0.1\ W_B$). In this case, the charge from $Q^* = 80\%$ to $Q^* = 95\%$ is about 5.5 hours. In winter – $t_{45} = (t_5 - t_4) = 2.5$ h, in summer – $t_{45} = 4$ h. Thus, it is necessary to ensure the value Q^*_4 in winter $Q^*_4 \geq 91\%$, in summer – $Q^*_4 \geq 87\%$.

It is possible to exclude the consumption of energy from the DG in the interval (t_3, t_4) under the condition:

$$W_{PV34}\eta_C \geq \left(W_{L34} + 0.01\frac{\left(Q^*_4 - Q^*_3\right)W_B}{\eta_C\eta_B} \right) \tag{3}$$

TABLE 1. *Charging SB characteristic with discreetness 0.5 hour*

Q^*_I, %	80	83.75	85	86.88	88.5	89.9	91	92	92.82	93.57	94.3
Q^*_{i+1}, %	83.75	85	86.88	88.5	89.9	91	92	92.82	93.57	94.3	95
I_{BAV}, p.u	0.075	0.045	0.0375	0.0325	0.0275	0.0225	0.0188	0.0163	0.015	0.014	0.013
ΔQ^*, %	3.75	2.25	1.88	1.62	1.375	1.125	0.94	0.82	0.75	0.7	0.65
P_B, p.u	0.375	0.225	0.188	0.162	0.137	0.113	0.094	0.082	0.075	0.07	0.065

If $W_{PV23} \leq W_{PVm0}$ even in the absence of generation to the grid, it is problematic to ensure the consumption of LO. Therefore, to limit the energy consumption for SB charging at night, during the morning peak it is possible to reduce Q^*_3 to 60% while limiting $Q^*_2 \leq 90\%$.

If condition (3) is fulfilled on the interval (t_3, t_4) dips are possible when $P_{PV}\eta_C < P_L$ and the missing energy is consumed from the DG. To reduce the consumption of electricity from the DG, it is advisable to exclude the SB charge, which will also ensure better use of the PV energy at other intervals. This is especially true in the case when a sharp decrease of the PV generation occurs at noon and the SB charge current is large enough. If $Q^* < 80\%$ then the SB charging current $I_B = 0.1\,C_B$, respectively, the power consumed to charge the SB $P_B = 0.1$, $W_B = 275$ W, and exceeds the load power. If the excess according to condition (3) is of the order of 5-10%, one should take into account the possible regulation of P_{PV} at intervals when $P_{PVP}\cdot\eta_C > P_L + P_B (P_B = U_B I_B / \eta_C\eta_B)$ and the actual value $P_{PVF} < P_{PVP}$ (P_{PVP} is the predicted value). In this case, a stock is entered with an overestimation of the value $Q^*_3 = 72\%$. We should also take into account possible deviations of P_L from the calculated value and P_{PVF} from the P_{PVP} forecast.

The algorithm of SB charge control is realized so. According to the $P_{PVP}(t)$ forecast on the next day (before the start of the night SB charge), the degree of charge is set depending on the W_{PV23} value (table 2) with a preliminary estimate of P_{g1}. Condition (3) is also checked and, if necessary, an overestimation of Q^*_3 is introduced.

TABLE 2. *Setting the SB charge degree*

W_{PV23}, W	$W_{PV23} \le 153$	$153 \le W_{PV23} \le 376$	$376 \le W_{PV23} \le 635$	$635 \le W_{PV23} \le 900$	$900 \le W_{PV23} \le 1200$	$1200 \le W_{PV23}$
Q_2^*, %	90	90	85	80	85	90
Q_3^*, %	60	70	70	70	70	70

At the moment $t_i = t_2$, according to the current forecast $P_{PVP}(t)_i$ and the measured value Q_{2i}^*, the reference P_{g1i} is refined. In this case, if P_{PVFi} differs from P_{PVPi}, the forecast is adjusted $W_{PV23i} = (P_{PVFi} / P_{PVPi}) W_{PV23}$. At the moment $t_{i+1} = t_2 + \Delta t$ (Δt is the discreteness of the forecast), according to the current forecast, W_{PV} generation is calculated on the interval (t_{i+1}, t_3), adjusted for the actual value of P_{PVFi+1}. Taking into account the average power value in the previous interval P_{Li} and $Q_{2(i+1)}^*$, the reference P_{g1i+1} is calculated. This is carried out until the moment t_3, when on the current forecast the generation W_{PV34} is calculated on the (t_3, t_4) with correction based on the actual value of P_{PVF3}.

The condition (3) is checked in accordance with W_{PV34} value, average value P_L on the previous interval and actual value Q_3^*. Based on this, a decision is made on the possibility of excluding the SB charge in case of generation dips in the interval (t_3, t_4). If (3) is not satisfied, at $P_{PV}\eta_C < P_L$ the SB is charged from the grid with the reference $I_B = 0.1\, C_B$. SB charge at intervals (t_1, t_2), (t_6, t_7) is not used at the daily tariff ($I_B = 0$).

The control system of converter unit is made according to well-known principles [10]. The functions of data processing, setting of modes and control of switching in the structure are performed by the program control unit (PCU). Communication with the site and conversion of the format of the received data $P_{PVP}(t)$ is carried out by the Wi-Fi module. Main operation modes:

- GM – operation in parallel with DG and with SB charge. If $P_{PV}\eta_C > P_L$, PV generation is regulated by maintaining the voltage in dc link U_d = const, the DG reference current amplitude i_g is set by $I_{gm}^1 = 0$, the SB reference $I_B = (P_{PV}\eta_C - P_L)/U_B$. If $P_{PV}\eta_C < P_L$, PV generation is maximum (set by the MPPT controller), reference SB current $I_B = I_{BR}$ and reference I_{gm}^1 is determined by the condition U_d = const. At condition (3) – $I_B = 0$;
- GM1 – operation with DG and energy generation $P_g \ge 0$ in the peak hours. PV works on the mode of maximum power, reference $I_{gm}^1 = 0$ or $I_{gm}^1 > 0$ (is determined by P_g value) sets the PCU according to the W_{PV23} forecast. Stabilization of voltage U_d is provided by regulation of SB current.

Simulation model for the study of energy processes in the system in the daily cycle

It implements the daily cycle of the PES operation without taking into account transients. Energy losses are taken into account through the efficiency. The operation of PES is considered with the use of various tariff plans. The model structure contains:

- module of PV generation forms $P_{PVP}(t)$ in accordance with forecast (archive data [13]) in tabular form, with PV generation regulation $P_{PV} = P_L + P_B$;
- module of estimation (EM) of the cost of paying for electricity consumption from DG;

- module of reference modes form variable, corresponding to time intervals. For summer period: *d* (day *d* = 1 from 7.00 to 8.00, from 11.00 to 20.00, from 23.00 to 24.00); *m* (morning load peak *m* = 1 from 8.00 to 11.00); *p* (evening load peak *p* = 1 from 20.00 to 23.00); *n* (night *n* = 1 from 24.00 to 7.00). For winter period intervals is shifted. The variables *gm*, *gm*1 is also formed for operating modes;
- load module with reference of load power $P_{LR}(t)$ in tabular form. In this case the value $P_L^1(t) = P_L(t) + P_g(t)(P_g(t) = P_{g1}m + P_{g2}p)$ is used in calculations;
- calculation module – calculates I_B, $P_B = I_B \cdot U_B$, power, consumed from DG P_g for GM, if $P_{PV}\eta_C < P_L$ then $P_g = P_L - P_{PV}\eta_C + P_B / \eta_C$ in night mode $P_g = P_L + P_B / \eta_C$.

SB model is made on data sheet. SB charge with energy taking account:

$$Q = Q_S + \int I_B^1 \cdot dt$$

where $I_B^1 = I_B \cdot \eta_B$ – when charge and $I_B^1 = I_B / \eta_B$ – when SB discharge.

I_B value is formed as $I_B(Q^*)$ in accordance with SB characteristics [14].

A "Saturation dynamic" unit is used with an upper limit $I_B(Q^*)$, and a lower one – $I_{Brc\max}$ (permissible value during discharge). The SB voltage is also set by the $U_B(Q^*)$ relationship.

EM calculates coefficient $k_E = C_1 / C_2$ [9] (C_1 is the cost of electricity consumed by the LO load at single tariff zone, C_2 is the cost of electricity consumed from the DG at the adopted tariff plan).

Results of simulation in MatLab

The model uses a PV with P_{PVR} = 1 kW, SB with W_B = 2.75 kWh, values $\eta_B = \eta_C$ = 0.94. The load $P_L(t)$ is in all cases unchanged with an increase in the evening peak in winter. The values of the degree of charge Q^*, the relative values of the generation power to the grid P_g and the values of k_{E1} (at single tariff rate), k_{E21} (at two tariff zones: day – 1, night – 0.5), k_{E31} (at three tariff zones: day – 1, night – 0.4, peak – 1.5) are given in table 3.

The oscillograms of the daily cycle of the PES operation for 1 July, 2015 at W_{PV} = 3.367 kWh with a sharp decrease of generation after lunch without SB charge form the grid is shown in figure 2. Margin (3%) for Q_3^* = 73%, Q_2^* = 86%, Q_6^* = 60%, k_{E1} = 4.132 is introduced (with connection to the grid under the same conditions k_{E1} = 2.97).

The oscillograms of the PES daily cycle for 28 July, 2015 at W_{PV} = 2.674 kWh with a sharp decrease of the PV generation in the morning and a SB charge at noon is shown in figure 3a (k_{E1} = 1.8). The dotted line highlights the fragments where the PV energy is not fully used (red), as well as the energy consumption for SB charging (blue), which is inappropriate. The exclusion of the SB charge (fig. 3b) provided an increase the use of the PV energy at k_{E1} = 2.15. The oscillogram for the clear day of December is shown in figure 4 at W_{PV} = 1716 Wh. P_{g1} = 75 W, P_{g2} = 40 W, Q_2^* = 80%, Q_3^* = 70%, Q_6^* = 50%, k_{E1} = 1.548, k_{E21} = 2.18, k_{E31} = 2.64.

TABLE 3. k_E value for different tariff plans

W_{PVP}, kWh	k_{E1}	k_{E21}	k_{E31}	Q_2^*, %	Q_3^*, %	Q_7^*, %	$\frac{P_{g1}}{P_L}$, %	$\frac{P_{g2}}{P_L}$, %
May-July (2015)								
6	14.66	+	+	90	70	63.3	204.8	33.3
6	13.73	+	+	80	70	63.4	152.4	33.3
6	20.3	+	+	80	70	60	152.4	47.6
4.756	6.29	+	+	85	70	63	142.8	33.3
4.756	7.39	+	+	85	70	60	142.8	47.6
4.346	6.56	+	+	85	70	62.5	143	33.3
3.751	3.167	6.32	19.3	85	70	61.9	57.1	33.3
3.367	4.132	12.21	+	86	73	60	162	33.3
2.83	2.36	3.76	5.58	85	70	61.4	33.3	33.3
2.83	2.33	4	7.13	90	70	61	57.1	33.3
2.674	2.15	3.5	5.12	90	60	60	33.3	33.3
2.021	1.733	2.37	3.43	85	70	63	85.7	33.3
1.951	1.66	2.2	2.79	82	70	62	47.6	33.3
December								
1.716	1.548	2.18	2.64	80	70	50	35.7	19
0.75	1.11	1.376	1.54	80	60	53	38.1	19
0.75	1.11	1.376	1.54	80	69	54	0	19

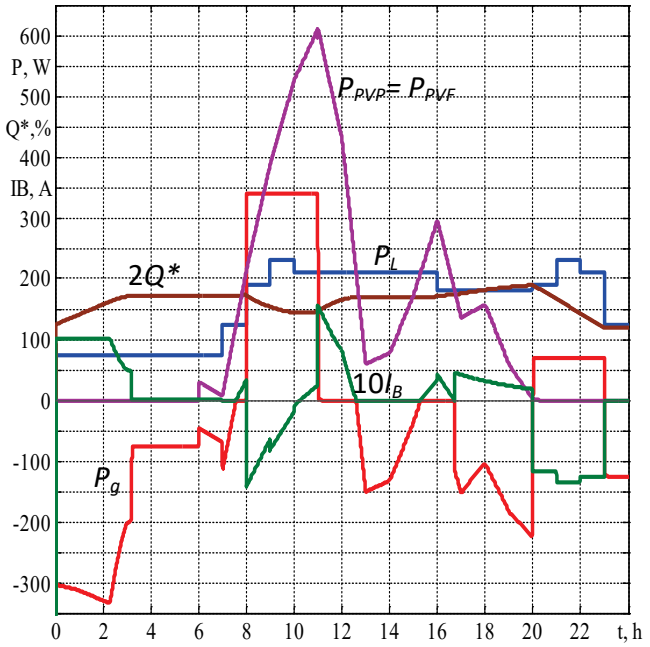

FIGURE 2. Oscilograms of PES daily cycle at W_{PV} = 3.367 kWh

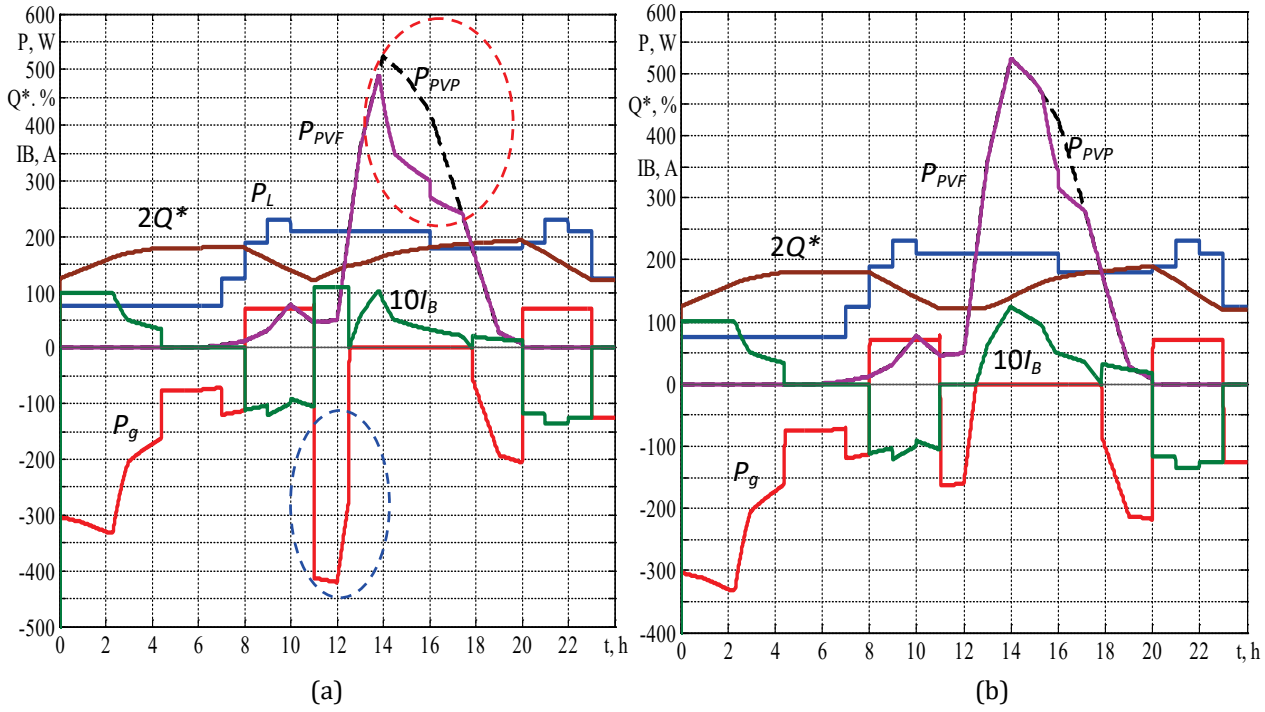

FIGURE 3. *Oscillograms of the PES daily cycle at W_{PV} = 2.674 kWh: a) with SB charge at noon; b) with the exclusion of the SB charge*

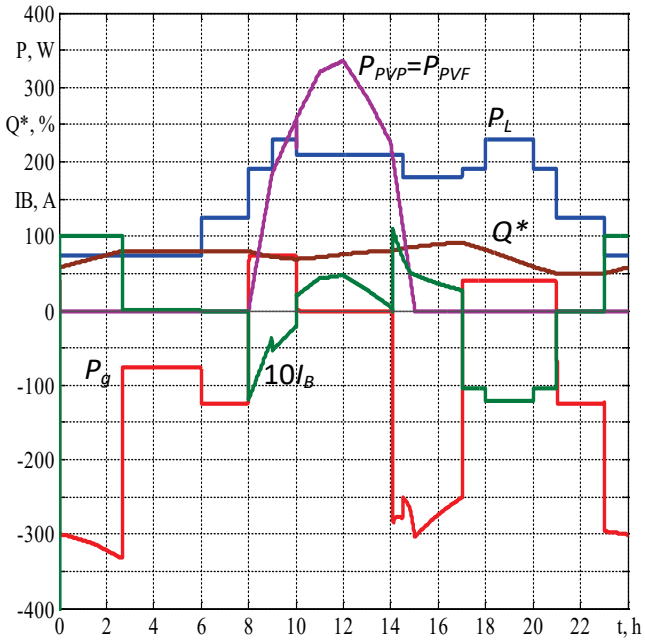

FIGURE 4. *Oscillogram of the PES daily cycle at W_{PV} = 1.716 kWh*

Conclusions

The proposed principles of the formation of the SB charge degree based on the prediction PV generation at the intervals of the PES operation ensure the planned uniform in time generation of electricity into the grid during peak hours. This is achieved while reducing energy consumption from the grid. The elimination of the SB charge in case of a sharp decrease in the PV generation allows you to reduce energy consumption from the grid with a more complete use of the PV energy. At the same time, the operation of the control system with the implementation of various operating modes is tied to tariff zones, the reference of the SB charge current and the value of the generation power is carried out by a program control unit with a Wi-Fi module.

Simulation in a daily cycle showed that with the adopted ratios of the PV power, SB capacity and load power, a decrease in the cost of paying for electricity from the grid at a single tariff zones by two or more times is possible when the power of the PV generation is more than 0.5 of the maximum value on a clear day. The exclusion of the SB charge in case of a sharp decrease in the PV generation provides a cost reduction up to 1.39 times at a single tariff rate. The value of the generation power to the grid during the morning peak for a clear day can be 2 times higher than the load power. The most efficiency is achieved with multi-zone billing. In winter, on cloudy days, the efficiency is expectedly low regardless of the tariffication.

References

[1] Conext SW. Hybrid Inverter, available: https://www.se.com/ww/en/product-range-presentation/61645-conext-sw/.

[2] ABB solar inverters. Product manual REACT-3.6/4.6-TL (from 3.6 to 4.6 kW), available: www.abb.com/solarinverters.

[3] Guerrero-Martinez M.A., Milanes-Montero M.I., Barrero-Gonzalez F., Miñambres-Marcos V.M., Romero-Cadaval E., Gonzalez-Romera E., *A Smart Power Electronic Multiconverter for the Residential Sector*, Sensors, 2017, 17(6), 1217, doi:10.3390/s17061217.

[4] Roncero-Clemente C., González-Romera E., Barrero-González F., Milanés-Montero M.I., Romero-Cadaval E., *Power-flow-based Secondary Control for Autonomous Droop-controlled AC Nanogrids with Peer-to-Peer Energy Trading*, in IEEE Access, Vol. 9, 2021, pp. 22339-22350, doi: 10.1109/ACCESS.2021.3056451.

[5] Shavelkin A.A., Gerlici J., Shvedchykova I.O., Kravchenko K., Kruhliak H.V., Management of power consumption in a photovoltaic system with a storage battery connected to the network with multi-zone electricity pricing to supply the local facility own needs, Electrical Engineering and Electromechanics, 2021, No. 2, pp. 36-42, doi: https://doi.org/10.20998/2074-272X.2021.2.

[6] Shavolkin O., Shvedchykova I., Improvement of the Three-Phase Multifunctional Converter of the Photoelectric System with a Storage Battery for a Local Object with Connection to a Grid, Proceedings of 2020 IEEE Problems of Automated Electrodrive, Theory and Practice (PAEP), Kremenchuk, Ukraine 2020, pp. 1-6, doi: 10.1109/PAEP49887.2020.9240789.

[7] Forecast. Solar, available: https://forecast.solar/.

[8] *SolarCast – an open web service for predicting solar power generation in smart homes*, Proceedings of the 1st ACM Conference on Embedded Systems for Energy-Efficient Buildings, November 2014, pp. 174-175, https://doi.org/10.1145/2674061.2675020.

[9] Shavolkin O., Shvedchykova I., Jasim J.M.J., *Improved control of energy consumption by a photovoltaic system equipped with a storage device to meet the needs of a local facility*, Eastern-European Journal of Enterprise Technologies, 2021, 2 (8 (110)), pp. 6-15, doi: https://doi.org/10.15587/1729-4061.2021.228941.

[10] Shavolkin O., Shvedchykova I., *Improvement of the multifunctional converter of the photoelectric system with a storage battery for a local object with connection to a grid*, Proceedings of 2020 IEEE KhPI Week on Advanced Technology (KhPIWeek), Kharkiv, Ukraine 2020, pp. 287-292, doi: 10.1109/KhPIWeek51551.2020.9250096.

[11] Traore A., Taylor A., Zohdy M.A., Peng F.Z., *Modeling and Simulation of a Hybrid Energy Storage System for Residential Grid-Tied Solar Microgrid Systems*, Journal of Power and Energy Engineering, 2017, No. 5, pp. 28-39, https://doi.org/10.4236/jpee.2017.55003.

[12] Sotnyk I.M., Zavdovyeva Y.M., Zavdovyev O.I., *Multi-rate Tariffs in the Management of Electricity Demand*, Mechanism of Economic Regulation, 2014, No. 2, pp. 106-113.

[13] Photovoltaic geographical information system, available: https://re.jrc.ec.europa.eu/pvg_tools /en/tools.html#SA.

[14] OPzV12-100 (12V100Ah) HENGYANG RITAR POWER CO., LTD, available: www.ritarpower.com.